Bioaccumulation and molecular effects of carbamazepine and methylmercury co-exposure in males of Dreissena polymorpha

Clément Baratange, Hugo Baali, Véronique Gaillet, Isabelle Bonnard, Laurence Delahaut, Jean-Charles Gaillard, Dominique Grandjean, Stéphanie Sayen, Andrea Gallorini, Nathalie Le Bris, et al.

Bioaccumulation and molecular effects of carbamazepine and methylmercury co-exposure in males of *Dreissena polymorpha*

Clément Baratange[1], Hugo Baali[1], Véronique Gaillet[1], Isabelle Bonnard[1], Laurence Delahaut[1], Jean-Charles Gaillard[2], Dominique Grandjean[3], Stéphanie Sayen[4], Andrea Gallorini[5], Nathalie Le Bris[6], David Renault[6,7], Florian Breider[3], Jean-Luc Loizeau[5], Jean Armengaud[2], Claudia Cosio[1*]

[1] Université de Reims Champagne-Ardenne, UMR-I 02 INERIS-URCA-ULH SEBIO, Unité Stress Environnementaux et BIOsurveillance des milieux aquatiques (SEBIO), BP 1039, F-51687 Reims Cedex, France.

[2] Université Paris-Saclay, CEA, INRAE, Département Médicaments et Technologies pour la Santé (DMTS), SPI, F-30200 Bagnols-sur-Cèze Cedex, France.

[3] Ecole Polytechnique Fédérale de Lausanne (EPFL), ENAC, IIE, Central Environmental Laboratory, Station 2, 1015 Lausanne, Switzerland.

[4] Université de Reims Champagne-Ardenne, Institut de Chimie Moléculaire de Reims (ICMR), UMR CNRS 7312, BP 1039, F-51687 Reims Cedex 2, France.

[5] Department F.-A. Forel for Environmental and Aquatic Sciences, and Institute for Environmental Sciences, University of Geneva, Boulevard Carl-Vogt 66, 1211, Geneva 4, Switzerland.

[6] Université de Rennes, CNRS, EcoBio (Ecosystèmes, biodiversité, évolution) - UMR 6553, F-35000 Rennes, France

[7] Institut Universitaire de France, 1 rue Descartes, 75231 Paris Cedex 05, France.

*Corresponding author: claudia.cosio@univ-reims.fr

Abstract

Dreissena polymorpha is a bivalve promising for biomonitoring in freshwater ecosystems thanks to its abundance and high filtration activity allowing rapid uptake of toxicants and identification of their negative effects. Nonetheless, we still lack knowledge on its molecular responses to stress under realistic scenario, *e.g.* multi-contamination. Carbamazepine (CBZ) and Hg are ubiquitous pollutants sharing molecular toxicity pathways, *e.g.* oxidative stress. A previous study in zebra mussels showed their co-exposure to cause more alterations than single exposures, but molecular toxicity pathways remained unidentified.

D. polymorpha was exposed 24h (T24) and 72h (T72) to CBZ (6.1±0.1 µg L^{-1}), MeHg (430±10 ng L^{-1}) and the co-exposure (6.1±0.1 µg L^{-1} CBZ and 500±10 ng L^{-1} MeHg) at concentrations representative of polluted areas (~10x EQS). RedOx system at the gene and enzyme level, the proteome and the metabolome were compared. The co-exposure resulted in 108 differential abundant proteins (DAPs), as well as 9 and 10 modulated metabolites at T24 and T72, respectively. The co-exposure specifically modulated DAPs and metabolites involved in neurotransmission, *e.g.* dopaminergic synapse and GABA. CBZ specifically modulated 46 DAPs involved in calcium signaling pathways and 7 amino acids at T24. MeHg specifically modulated 55 DAPs proteins involved in the cytoskeleton remodeling and hypoxia-induced factor 1 pathway, without altering the metabolome. Single and co-exposures commonly modulated proteins and metabolites involved in energy and amino acid metabolisms, response to stress and development. Concomitantly, lipid peroxidation and antioxidant activities were unchanged, supporting that *D. polymorpha* tolerated experimental conditions.

The co-exposure was confirmed to cause more alterations than single exposures. This was attributed to the combined toxicity of CBZ and MeHg. Altogether, this study underlined the necessity to better characterize molecular toxicity pathways of multi-contamination that are not predictable on responses to single exposures, to better anticipate adverse effects in biota and improve risk assessment.

Keywords: bivalve, freshwater, multi-omics, toxicity pathways

1. Introduction

In the context of environmental contamination, biomonitoring aims to assess environmental health to protect biota and linked ecosystem services. The zebra mussel *Dreissena polymorpha* (Pallas, 1771) is promising for freshwater biomonitoring and ecotoxicological studies (Kerambrun et al., 2016; Klimova et al., 2017; Louis et al., 2019, 2020; Hani et al., 2021; Baratange et al., 2022). This species is widely distributed, abundant, and sessile. Its high filtration activity results in the bioaccumulation of pollutants triggering biological responses that can be measured (Binelli et al., 2015). Nonetheless, a better understanding of the physiology of this mussel is a prerequisite for its efficient use in biomonitoring.

Recent omics techniques opened new research perspectives in stress biology and ecotoxicology, particularly in non-model biota (Gonzalez and Pierron, 2015; Gouveia et al., 2019). Proteomics and metabolomics identified molecular targets, molecular toxicity pathways of pollutants, and potential biomarkers relevant for biomonitoring (Armengaud et al., 2014; López-Pedrouso et al., 2020; Dumas et al., 2022a). Combining multi-omics approaches and targeted endpoints at different biological organization levels gives a holistic view of responses and appears particularly powerful to identify molecular toxicity pathways of pollutants (Brinke, 2017; Gouveia et al., 2019; Dumas et al., 2022a).

Here, we investigated molecular toxicity pathways of two ubiquitous pollutants in aquatic ecosystems: mercury (Hg) and carbamazepine (CBZ) (Andreu et al., 2016). CBZ is an anti-epileptic drug without European legislation, but Germany and the Netherlands recommended an environmental quality standard (EQS) of 0.5 µg L^{-1} (EC, 2010; Kase, 2010; ETOX, 2011). Due to its limited biodegradation and elimination by wastewater treatment plants (Zhang et al., 2008; Calisto et al., 2011), CBZ is ubiquitous and was proposed as an indicator of the level of anthropogenic activities (Clara et al., 2004; Dvory et al., 2018). It reached up to 10 µg L^{-1} in freshwaters (Verlicchi et al., 2012). Concentrations are expected to increase in the future, because of its wide use in human and veterinary medicine (Oldenkamp et al., 2019). The mode of action of CBZ in vertebrates was

74 suspected to target ion channels (Ambrósio et al., 2002). In bivalves, CBZ exposure triggered
75 oxidative stress, defense responses and altered the energy metabolism at 1-10 µg L^{-1} range (Chen et
76 al., 2014; Almeida et al., 2015; Baratange et al., 2022; Dumas et al., 2022b, Baali and Cosio, 2022).
77 CBZ at 5 µg L^{-1} caused a delayed spermatogenesis in *D. polymorpha* (Magniez et al., 2018), suggesting
78 reprotoxicity.

79 Hg is a metal ubiquitous in aquatic ecosystems due to natural and anthropogenic sources. It is
80 included in the European list of priority pollutants (Directive 2008/105/EC) and targeted by the
81 Minamata International Convention (Reg. EC 1881/2006; http://mercuryconvention.org/). The
82 current EQS in Europe is 70 ng L^{-1} of total Hg (Directive 2008/105/EC). Recently, up to 1-8 µg L^{-1},
83 representing more than 100x EQS, were reported in aquatic environment (Mahat et al., 2018; Zhou
84 et al., 2018). Hg occurs mainly as inorganic Hg (IHg; HgII) or methylmercury (MeHg; CH_3HgII) forms in
85 the aquatic environment. IHg in 10-30 µg L^{-1} range was reported to cause oxidative stress, alter
86 energy metabolism and defense responses in bivalves (Liu et al., 2011; Velez et al., 2016; Coppola et
87 al., 2017). IHg-contaminated algae modulated seven proteins involved in reproductive function of
88 *Crassostrea angulata*, suggesting reprotoxicity (Zhang et al., 2013). However, MeHg toxicity is of
89 most concern due to its biomagnification in food webs (Kershaw and Hall, 2019) and lower
90 depuration than IHg (Metian et al., 2020). In vertebrates, MeHg exposure resulted in alterations of
91 the nervous system and cytoskeleton (Yadetie et al., 2016; Pierozan et al., 2017). In gills of *D.*
92 *polymorpha,* exposure to 280 ng L^{-1} MeHg 7d caused antioxidant responses and cellular damages
93 (Baratange et al., 2022).

94 CBZ and Hg have been found in common sites in aquatic environments (*e.g.* Zhang et al., 2017).
95 Both alter similar molecular toxicity pathways in biota. Their co-exposure in *D. polymorpha* caused
96 more effects than single exposures (Todgham and Stillman, 2013; Baratange et al., 2022). Besides,
97 effects observed in the co-exposure were unpredictable based on the bioaccumulation and effects
98 caused by single exposures (Baratange et al., 2022). In this context, a better insight into the

molecular toxicity pathways of CBZ and Hg in single and co-exposures is needed for a better anticipation of adverse effects in complex exposure scenarios. Because gender modulates responses (Ji et al., 2013, Ji et al., 2014), we exposed males of *D. polymorpha* to CBZ, MeHg and their co-exposure at nominal concentrations representative of polluted areas (10x EQS; 5 µg L^{-1} and 700 ng L^{-1}, respectively), tolerated by *D. polymorpha* in previous analysis (Baratange et al., 2022). We analyzed biological responses using untargeted proteomics at 24h (T24) combined with targeted metabolomics, antioxidant responses at gene and protein levels, lipid peroxidation and pollutant bioaccumulation at T24 and 72h (T72), to account for kinetics response that might differ among the different organization levels spanning gene expression to metabolites. We performed a short exposure to gain knowledge on the mode of action and the molecular toxicity targets of CBZ, MeHg and the co-exposure in *D. polymorpha*.

2. Material and methods

2.1. *Dreissena polymorpha* collection and acclimation

About 1,000 individuals of *D. polymorpha* were collected from the "Lac du Der-Chantecoq" (Marne, France; 48° 36' 22.02" N, 4° 46' 34.0" E) in February 2020. Individuals of 22-28 mm-long were sorted and cleaned. Mussels were depurated one week in an aquarium filled with 9 L of spring water (Cristaline Aurèle, table S1) in darkness at 12 °C, corresponding to the field temperature when collected. Puncture with a syringe in gonads of 0.1 to 0.2mL was observed by microscopy (x200) to observe gametes, determine sex and select males. The index of sexual maturity (ISM) was determined on dissected gonad (n = 10) by flow cytometry as described in Magniez et al. (2018): 60% were in the pre-spawning stage (ISM = 3.5 to 4.7) and 40% in gametogenesis (ISM = 2.5 to 3.5), with an average ISM of 3.6 ± 0.2. 360 males were acclimated at 12 °C in darkness for two weeks in 9 L of local spring water. Males were randomly dispatched into 8 aquaria with 45 individuals per aquarium and 3.375 L of spring water and further kept in darkness at 12°C for 7d. During this acclimation,

mussels were fed with *Nannochloropsis spp.* (Nanno 3600, Instant Algae) using $2 \cdot 10^6$ of algal cells per individual per day. Water was continuously aerated (> 80% O_2) and renewed twice a week.

2.2. Experimental design

Temperature, feeding and mussel density used during acclimation were maintained for exposures in semi-static conditions. Water was renewed and spiked daily or not (control, Ctl), with carbamazepine (CBZ), methylmercury (MeHg) and the co-exposure CBZ+MeHg. Two aquaria were spiked for each exposure. One was analyzed at 24h (T24), and the other at 72h (T72). No mortality was recorded during the experiment.

The effective concentrations of CBZ and MeHg were determined by sampling and filtering (0.45 µm, Sterivex) 10 mL of water collected daily immediately after spiking (n=1 per tank and per timepoint). Temperature, pH, conductivity and oxygen concentration, nitrate, nitrite, and ammonium were respectively analyzed daily with a multimeter (MU 6100H, VWR) and by spectrophotometry following the manufacturer protocol (Permachem) in a sample of 50 mL water taken just before the water renewal (n=1).

At T24, five mussels were deshelled, snap-frozen in liquid nitrogen and stored at -80 °C for proteogenomics analyses. The other endpoints were analyzed at T24 and T72. For bioaccumulation analyses, 9 mussels were deshelled, rinsed with spring water and the whole soft tissues kept at -80 °C. For metabolomics analyses, 8 mussels were frozen in liquid nitrogen and stored at -20 °C. For qPCR and biochemical analyses, 16 mussels were dissected, and digestive glands, gills and gonads frozen in liquid nitrogen and stored at -80 °C.

2.3. Pollutant analysis

2.3.1. Carbamazepine

148 Water aliquots were frozen until analysis. Samples were 10x enriched through centrifugal
149 vacuum evaporation at 37 °C using a Genevac HT Series (SP Scientific). This preparation step was
150 validated using CBZ standards and control solutions that were systematically concentrated in parallel
151 to samples. A High-Performance Liquid Chromatography (HPLC) system (Agilent technologies, 1260
152 Infinity), consisting of a quaternary pump and a photodiode array detector, allowed the measure of
153 CBZ concentrations from water samples. To elute the analytes (20 µL), a mobile phase containing
154 acetonitrile (A) and ultra-pure water (ALPHA Q 18.2 MΩ cm^{-1}) with orthophosphoric acid (0.1%) (B)
155 was used on a reverse-phase Agilent Pursuit XRs 5 C_{18} column (5 µm x 250 x 3 mm) at 20 °C. CBZ was
156 measured at 214 nm after the elution at a flow rate of 0.80 mL min^{-1} in gradient condition from
157 35/65% to 100/0% (v/v) A/B. Analyses were performed in triplicate.
158 Soft tissues were freeze-dried (48h at 0.3 mbar; Vacuubrand GMBH) and grinded for 8min at
159 30 Hz (MM400, Retsch) with one 8 mm stainless steel bead. After weighing, the dry tissue was
160 resuspended in 10 mL acetonitrile, 200 µL n-heptane and 2.5 mL ammonium acetate (0.4 M). The
161 supernatant was recovered by centrifugation (1,620 g, 10min), concentrated under nitrogen flux
162 evaporation at 40 °C, resuspended in the eluent solution, and 10 µL of the samples injected into the
163 UPLC-MS/MS (Acquity UPLC Xevo TQ-MS system, Waters). The concentration was determined for
164 each sample by using a standard curve from 0.5 to 12 ng mL^{-1} CBZ, and by adding an internal
165 standard of 50 ng mL^{-1} CBZ-d_{10} in the samples. The quality of the analyses was validated by analyzing
166 blanks.

167

168 2.3.2. Methylmercury

169 Water aliquots were acidified with 0.5% v/v HCl (Suprapur, Merck), and kept at 4 °C until
170 analyzed. Whole soft tissues were freeze-dried, weighed and ground for 8min at 30 Hz (MM400,
171 Retsch) by an 8 mm stainless steel bead and digested in 30% v/v HNO_3 (Suprapur, Merck) for 12h at
172 60 °C. MeHg concentration was analyzed by MERX-M (Brooks Rand Instruments) following MeHg

procedure (US EPA 1630, 2001). The analytical quality was validated by analyzing blanks and certified reference materials (DORM-4, TORT-2; NRC – CNRC).

2.4. Shotgun proteomics

2.4.1. Data acquisition

Whole soft tissues were freeze-dried and grinded by bead-beating with two 2 mm-diameter steel beads in a Precellys instrument (Bertin) operated for 3 times 20s at 5,000 rpm. The powder was pelleted by centrifugation for 1min at 1,500 g, weighted, and dissolved in 12.5 µL of LDS1X (Thermo) per mg of powder. The mixture was subjected to bead-beating for 6 cycles of 20s at 7,200 rpm, followed by 30s of ultrasonication with a Hielscher UP50H sonicator operated at 90% amplitude, and then 4 cycles of bead-beating at 6,500 rpm. Each sample was centrifuged for 3min at 10,000 g to eliminate debris and the resulting supernatant was diluted by 7 volumes of LDS1X. After denaturation of the proteins for 5min at 99 °C, 30 µL were subjected to denaturing electrophoresis on a NuPAGE 4-12% gradient gel ran in MES buffer (Thermo) for 5min as recommended (Hartmann et al., 2014). Each proteome was processed as a single polyacrylamide gel slice and proteolyzed with trypsin (Promega) in presence of 0.01% ProteaseMAX surfactant (Promega) as described by Hartmann et al. (2014). The resulting peptides (2 µL out of 50 µL) were analyzed with a Q-Exactive HF mass spectrometer (Thermo) operated in data-dependent mode using parameters previously described (Klein et al., 2016). Peptides were resolved on an Acclaim PepMap100 C18 (3 µm, 100 Å, 75 µm id x 50 cm) at a flow rate of 0.2 µL per min along a 90 min gradient of acetonitrile in presence of 0.1% formic acid (3.2%-20% in 75min and then 20%-32% in 15min). A dataset of 1,472,640 high-resolution MS/MS spectra was recorded. The dataset was queried with the MASCOT software (MatrixScience) in follow-up mode against two complementary databases: a RNA-seq derived database named Dreissena_HJ1_pep_20170801.fasta, and then the Dreissena_polymorpha_Cosio300seq_2020-11-11.fasta listing 300 additional protein sequences. A

protein was considered as significantly modulated if |TFOLD|≥1.40 and p-value<0.05. A total of 162 differential abundant proteins (DAPs) were detected when comparing pollutant exposures to the Ctl. The mass spectrometry and proteomics datasets acquired on samples are available through the ProteomeXchange Consortium via the PRIDE partner repository, with the dataset identifier PXD040345 and 10.6019/PXD040345 [The reviewers may access this currently private dataset using https://www.ebi.ac.uk/pride/ website with the username as reviewer_pxd040345@ebi.ac.uk and password as aRt4WSai] (tables S2 and S3).

2.4.2. Protein annotation and enrichment analyses

The dataset showed 2,722 proteins with at least seven spectral counts that were annotated by homology with the EggNOG v5.0 software (http://eggnog5.embl.de) using default parameters (auto adjust per query, transfer annotation from any ortholog, E-value threshold set at 10^{-3}, minimum of 40% identity and of 20% of query and subject coverage). Identified proteins were analyzed with Kyoto Encyclopedia of Genes and Genomes (KEGG) pathway database and gene ontologies (GO) terms using WEB-based GEne SeT AnaLysis Toolkit (WebGestalt; http://www.webgestalt.org/) for enrichment analysis (table S4), as it offers the possibility to use our dataset of 2,722 proteins as background list. To identify the most relevant KEGG pathways or GO terms, redundancy reduction was performed applying a weighted set cover (p-value<0.05, and ≥2 DAPs). Eventually, non-relevant pathways for *D. polymorpha* were removed from the output (*e.g.* fluid shear stress and atherosclerosis, ko05418). For each protein, the ratio of normalized spectral abundance factor (%NSAF) of KEGG pathways and GO terms was calculated as the sum of spectral counts in the five replicates normalized by its molecular mass in kDa divided by the sum of all NSAF values measured in the exposure condition as previously described (Christie-Oleza et al., 2012).

2.5. Targeted metabolomics

223 Freeze-dried soft tissues of animals were collected from shells and weighed. Then, metabolites
224 were extracted by adding a volume of 900 µL of a solution of ice-cold methanol / chloroform (2/1,
225 v/v), and the samples were homogenized with a bead-beater (Retsch TM MM301) with two tungsten
226 beads (3 mm diameter) in a 2 mL microtube. The extracts were kept at -20 °C overnight, grinded
227 again at 25 Hz for 90s. A volume of 600 µL of ultrapure water (18.2 MΩ cm^{-1}) was added in each
228 extract. After homogenization, samples were centrifuged (4,000 g, 10min, 4 °C), and the supernatant,
229 containing metabolites, was collected and kept at -20 °C until analyses.

230 Three different aliquots of 180, 120 or 90 µL were pipetted from samples having dry masses of
231 50 – 90 mg, 90 – 150 mg, and > 150 mg, respectively to reliably detect and quantify metabolites.
232 Extracts were transferred into 300 µL glass vials and dried for 1h at 32 °C (Genevac, miVac DNA). Dry
233 residues were resuspended in 30 µL of methoxyamine hydrochloride (Sigma-Aldrich, 25 mg L^{-1}) in
234 pyridine (Fisher chemical), and automatically homogenized at 40 °C for 60min, before adding 30 µL of
235 N,O-Bis(trimethylsilyl) trifluoroacetamide (BSTFA, Sigma-Aldrich) followed by incubation at 40 °C for
236 60min. A volume of 1 µL of the supernatant was injected in the Agilent 7890/5977B GC/MS platform.
237 We used the equipment and settings described by Thiébaut et al. (2021). Chromatograms were
238 established and analyzed using the software provided by the manufacturer (MS Quantitative
239 Analysis, Quant-My-Way, Agilent B09.00). Standard samples included 62 reference compounds at 1-
240 2-5-10-20-50-100-200-500-750-1,000-1,500 µM. Quadratic calibration allowed to accurately
241 annotate and quantify 31 metabolites in samples (tables S5, S6, S7).

242

243 2.6. Gene expression level

244 The relative gene expression level of catalase (cat), glutathione-s-transferase (gst), superoxide
245 dismutase (sod) and metallothionein (mt) was analyzed in digestive glands, gills and gonads using
246 actine (act) and ribosomal protein S3 (ps3) as reference genes (table S8). Digestive glands are
247 important detoxifying organs for chemical exposure, gills are directly exposed to the media, and

gonads are essential to ensure the species reproduction, *i.e.* for the survival. RNA was extracted with TRI Reagent (Euromedex) following the manufacturer protocol. Quality and quantity of RNA were determined by electrophoresis on 1% agarose gel in Tris Borate EDTA (TBE; 0.5%) buffer and with Nanodrop (Jenway). Reverse transcription (RT) was performed using 400 ng RNA with the verso cDNA synthesis kit (Thermo Scientific) and oligodT primers, with a PCR Mastercycle (Eppendorf) at 42°C for 1h followed by 3min at 95°C. Quantitative polymerization chain reactions (qPCR) were conducted with 3 µL of 1/10 diluted cDNA and Absolute Blue qPCR SYBR Green (Thermo Scientific), using a CFX96 automaton (BioRad; 95°C 15min, 40 cycles 95°C 10s, 60°C 45s) following the $2^{-\Delta\Delta Ct}$ method (Schmittgen and Livak, 2008).

2.7. Biochemical analyses

To distinguish targets of sections 2.6. and 2.7., thereafter gene expression levels are mentioned in lowercase, while enzyme activities are written in uppercase. We determined the protein concentration, GST activity, lipid hydroperoxides (LOOH) resulting from lipid peroxidation, CAT activity, SOD activity and MT abundance in digestive glands, gills and gonads as described in Baratange et al. (2022). Briefly, tissues were weighed and suspended (8/1 v/w) in phosphate buffer pH 7.4 (50mM, VWR), phenylmethylsulfonyl fluoride (PMSF 1mM, Sigma-Aldrich) and L-serine borate (1mM, Sigma-Aldrich) as protease inhibitors, grinded at 30 Hz for 90s three times by an 8 mm stainless steel bead and centrifuged 15min at 3,000g (4 °C). The supernatant (= homogenate) was collected and kept at -80 °C until analysis.

The automated spectrophotometer Gallery (Thermo Scientific) was used to determine the protein concentration, GST activity and LOOH. Protein concentration was measured at 600 nm after a 5min reaction by the colorimetric method of red Pyrogallol and 1/6 (v/v) of the homogenate, using calibration curve from bovine serum sCal (66.7 µg L^{-1}) diluted 50 to 200x and protein reagents U/CSF from the manufacturer (Thermo Scientific). GST activity was measured at 340 nm for 4min through

the conjugation of 0.9mM CDNB with 1mM reduced glutathione in 0.1M phosphate buffer pH 6.5, and 1/40 (v/v) of the homogenate. LOOH concentration was determined at 620 nm after a 30min reaction on 1/46 (v/v) of the homogenate, 139mM Fe II D-gluconate dehydrate and 240mM orange xylenol, in acidic solution of H_2SO_4 40mM, glycerol 1.37M, formic acid 20mM and NaCl 0.9%, with tert-butyl hydroperoxide (TBH) at 0.125, 0.25, 0.5, 1, 2, 4, 8 and 16µM for calibration.

CAT activity was measured by a spectrophotometer (Cary 50, Agilent, Australia) through the degradation of 14 mM H_2O_2 (Sigma-Aldrich) at 240 nm for 120s on 1/100 (v/v) of the homogenate for digestive glands, and 1/50 (v/v) of the homogenate for gills and gonads in 50mM phosphate buffer pH 7.4, using a calibration curve from purified bovine serum CAT at 1.25, 2.5, 5, 10, 15 and 20 U mL^{-1}.

SOD activity was measured by a spectrophotometer (Spark 10M, TECAN, Austria) after 20min reaction in darkness, at 340 nm for 30min on 1/85 (v/v) of the homogenate for digestive glands, and 1/43 (v/v) of the homogenate for gills and gonads, with 2.35mM EDTA dihydrate, 1.17mM $MnCl_2$, 1mM β-mercaptoethanol, 0.28mM β-NADH in 50mM phosphate buffer pH 7.4. The inhibition of β-NADH oxidation was followed, and activity was determined in the linear range, using a calibration curve from purified bovine serum SOD at 0.125, 0.25, 0.35, 0.5 and 0.7 U mL^{-1}.

MT concentration was measured with a polarograph (797 VA Computrace Metrohm) by sulfhydryl groups (-SH) determination, as described by Thompson and Cosson (1984). The homogenate was heat-shocked 15min at 75°C, kept 10min at 4 °C, centrifuged 10min at 15,000 g (4 °C), and the supernatant collected. Analyses were performed at 4 °C in a thermostated cell containing 10 mL Bridcka reagent, 150 µL of Triton solution, and 30 µL (digestive glands) or 60 µL (gonads) of the supernatant. Concentrations were determined using a calibration curve of 1, 2, 3, 4, 5, 6 µg standard MT from liver's rabbit (Sigma).

2.8. Data interpretation and statistical analysis

297 Data are presented as arithmetic mean ± standard error of the mean (SEM). A bioaccumulation
298 factor (BAF; L kg^{-1}) of MeHg and CBZ was calculated by dividing the concentration in mussels (µg kg^{-1})
299 by the effective concentration in water (µg L^{-1}). We applied two-way ANOVA analyses to test if
300 exposure and/or time significantly altered bioaccumulation, gene expression level, biochemical
301 responses and metabolome. We applied one-way ANOVA to test if exposure significantly altered
302 proteome in Rstudio software (v 4.0.3.; α = 5%; table S9). Normality and homoscedasticity of
303 residuals was checked by Kolmogorov-Smirnov's and Bartlett's tests, respectively. We considered a
304 biological effect if p-value<0.05, and the fold change (FC)≥1.20 and ≤0.83 for gene expression level
305 and biochemical analyses and FC≥1.40 and ≤0.71 for proteogenomic and metabolomic.

306 Venn diagram was performed with InteractiVenn (Heberle et al., 2015), while principal
307 component analysis (PCA) and partial least square discriminant analyses (PLS-DAs) were performed
308 using Metaboanalyst (www.metaboanalyst.ca). Heatmaps were constructed using Metaboanalyst to
309 cluster individuals with average method and measure of Euclidean distance. Pathway analyses on
310 modulated metabolites were performed with Metaboanalyst using KEGG database in October 2019
311 (p-value<0.05, and ≥2 metabolites).

312

313 **3. Results**

314 3.1. Water analyses

315 Effective concentrations of carbamazepine (CBZ; 6.1±0.1 µg L^{-1}), methylmercury (MeHg; 430±10
316 ng L^{-1}) and the co-exposure (6.1±0.1 µg L^{-1}CBZ; 500±10 ng L^{-1} MeHg) and control (Ctl) were stable
317 from the beginning to the end of the exposure (n=3) and represented 12x the recommended EQS for
318 CBZ (ETOX 2011) and 7x EQS for Hg in Europe (Directive 2008/105/EC; figure S1). Water analysis
319 showed stable chemical parameters with similar values for all exposures and time points:
320 temperature 12.1 ± 0.3 °C, pH 8.5 ± 0.1, conductivity 500 ± 20 µS cm^{-1}, oxygen saturation 75.8 ± 0.1 %

O_2, nitrates 9 ± 1 mg L^{-1}, nitrites 0.10 ± 0.02 mg L^{-1} and ammonium 0.04 ± 0.02 mg L^{-1} (figure S1). Consequently, responses described thereafter are attributed to the effect of pollutants.

3.2. Bioaccumulation

CBZ and MeHg in single and co-exposure at 24h (T24) and 72h (T72), showed a significant bioaccumulation (respectively: $p<2E^{-16}$ and $p=1.7E^{-6}$) and a similar BAF across time (respectively: p=0.511 and p=0.143) (figure 1). No difference was observed between single and co-exposure for CBZ (p>0.1) and MeHg (p>0.1), suggesting that differences show inter-individual variability. MeHg resulted in BAF 44x to 96x higher than CBZ. The other pollutant was not bioaccumulated in single exposures (p>0.1).

3.3. Proteogenomics

The whole proteome of mussels at T24 by shotgun proteomics and the MS/MS spectra was interpreted using a RNA-seq derived database. Sequences of 4,892 proteins identified with at least one peptide were grouped into the database MS20-032_ProtSpec_2020-11-27 which comprises a total of 2,224,933 amino acid residues. This database was queried, resulting in the final assignment of 838,587 MS/MS spectra (FDR 1%). In total, 32,918 unique peptide sequences at high confidence (FDR below 1%) were identified. These peptides showed the presence of 4,375 proteins with at least one specific peptide, and a total of 3,183 with at least two peptides (table S2). Their functional annotation was obtained by sequence similarity search (table S3).

An average of 21,410 spectral counts was measured per sample. A cut-off of >6 spectral count abundances was used to select 2,722 proteins in the dataset, including 2,477 proteins (91%) with at least one GO-term or one KEGG pathway. Compared to Ctl, CBZ, MeHg and the co-exposure respectively showed 46, 55 and 108 differential abundant proteins (DAPs) by univariate analyses,

suggesting that the co-exposure caused more alterations than single exposures. CBZ (85%), MeHg (95%) and their co-exposure (97%) showed mainly DAPs more abundant than in Ctl. Only 7 DAPs were common in all exposures (figure 2), indicating an increase of the biosynthesis of proteins specific to each experimental condition. In the same line, PCA analyses of the 162 DAPs in at least one exposure discriminated exposures along the first component explaining 33.5% of the variability, and pollutants were differentiated along the second component explaining 12.4% of the variability (figure 2). The highest increase and decrease in abundance of the 162 DAPs *vs* Ctl (log_2 fold change FC) were <2, indicating limited protein modulations by pollutants (table 1). Annotations of DAPs in all exposures included proteins involved in response to stress, signal transduction, transcription and translation processes. Other DAPs modulated to CBZ and MeHg single exposures were involved in cytoskeleton (*e.g.* spectrin) while MeHg single exposure and the co-exposure modulated DAPs involved in intracellular transport. This analysis also identified uncharacterized proteins (7.4%), underlining the need to gain knowledge on the biology and stress responses of *D. polymorpha*.

Enrichment analyses of KEGG pathways and GO-terms confirmed that the co-exposure CBZ+MeHg caused more alterations than single exposures in *D. polymorpha*, shown by a higher %NSAF and a higher number of DAPs per enriched pathway (figure 2). The co-exposure modulated DAPs involved in transcription processes (*e.g.* eukaryotic translation initiation factor 3 complex), intracellular transport, and signaling pathway such as MAPK (mitrogen activated protein kinases) cascade. CBZ exposure modulated DAPs involved in protein turnover (*e.g.* regulation of protein ubiquitination) and signal transduction, including the calcium signaling pathway. MeHg exposure modulated DAPs involved in cytoskeleton organization (*e.g.* barbed-end actin filament capping) and signaling pathway, including the hypoxia-inducible factor 1 (HIF-1) and Toll and Imd signaling pathways. All exposures modulated DAPs involved in amino acid metabolism, energy metabolism, cellular development, signal transduction and response to stress (figure 2). However, most enriched GO-terms and KEGG pathways were specific to each exposure, in congruence with the Venn diagram and PCA analysis (figure 2).

371

372 3.4. Targeted metabolomics

373 At T24, univariate analyses compared to Ctl showed that CBZ exposure resulted in significant
374 depletion of the amount of 5 metabolites, while the co-exposure resulted in a significant ~~increase~~
375 decrease of the concentration of one metabolite ($p<0.05$, figure 3, tables S4 and S5). Increase or
376 decrease in metabolite amounts in exposures compared to Ctl (log_2 FC) were ≤2.1, indicating limited
377 metabolite modulations in our experimental conditions (figure 3). At T72, no modulation was
378 measured.

379 A high individual variability (figure 3) could mask modulations of metabolites, thus limiting the
380 power of univariate approaches. Consequently, multivariate analyses were favored and will be
381 further discussed. PCA analyses did not discriminate metabolic profiles of exposures, hence PLS-DAs
382 were performed (figure 4). The metabolic profiles in both CBZ and the co-exposure were different
383 from Ctl at T24, and the latter at T72. These results further supported that the co-exposure triggered
384 more alterations than single exposures. At T24, CBZ and Ctl were mostly discriminated by component
385 1, while the co-exposure and Ctl were discriminated by component 2. Metabolites with a VIP
386 score>1.0 (*i.e.* most discriminant metabolites) and FC>1.4 suggested that CBZ and the co-exposure
387 resulted in the alteration of the concentration of 7 and 9 metabolites, respectively. At T72, the co-
388 exposure and Ctl were discriminated along components 1 and 2, with 10 metabolites modulated
389 compared to Ctl. At both timepoints, modulated metabolites were involved in aminoacyl-tRNA
390 biosynthesis ($p<0.01$), valine, leucine and isoleucine biosynthesis and degradation ($p<0.05$). CBZ
391 exposure at T24 caused the specific alteration of glycine, serine and threonine metabolism ($p<0.01$)
392 and biotin metabolism ($p<0.05$). The co-exposure at both timepoints caused the alteration of
393 pantothenate and CoA biosynthesis ($p<0.01$). At T24, the co-exposure altered alanine, arginine,
394 aspartate, glutamate, proline metabolism ($p<0.05$), arginine biosynthesis ($p<0.01$), and at T72
395 glycerolipid metabolism ($p<0.01$).

Omics and targeted analyses revealed molecular toxicity pathways triggered by single and co-exposures (figure 5). Single exposures and co-exposure at T24 and the co-exposure at T72 caused the modulation of amino acid metabolism, energy metabolism, and protein turnover. At T24, single and co-exposures altered the cellular development and response to stress. Globally, data confirmed that the co-exposure caused more alterations than single exposures.

3.5. Lipid peroxidation and defense responses

We analyzed defense responses at the gene and enzyme level and lipid peroxidation in digestive glands, gills and gonads. No significant modulation *vs* Ctl was evidenced ($p>0.05$; table 2), supporting that MT and defense background level in *D. polymorpha* were efficient to tolerate Hg in our experimental conditions.

3.6. Link of biological endpoints and pollutant bioaccumulation

In our experimental conditions, no obvious correlation of bioaccumulation with biological effects was observed in *D. polymorpha*: the co-exposure did not significantly change bioaccumulation ($p>0.1$), while proteomics and metabolomics showed a higher number of significant modulations *vs* Ctl.

4. Discussion

4.1. Specific molecular toxicity pathways

Carbamazepine (CBZ) exposure to concentration representative of contaminated areas caused a specific enrichment of proteins involved in the KEGG pathway “calcium signaling”. Similarly, in digestive glands of *Mytilus galloprovincialis*, exposure to 1 µg L^{-1} CBZ 28d resulted in a significant

420 modulation of the expression of genes involved in calcium ion binding, sodium ion transport, and
421 potassium channels (Mezzelani et al., 2021). In the same line, injection of 1 mg CBZ kg^{-1} in the fish
422 *Solea senegalensis* caused an increase of up to 3x of Na^+, K^+-ATPase activity and 1.1x osmolality at
423 48h, supporting an alteration of osmoregulation (Seifter and Chang, 2017; González-Mira et al., 2016,
424 2018). Because ion balance is instrumental to maintain osmotic homeostasis, their modulation may
425 result in alterations of osmoregulation and cellular homeostasis (Seifter and Chang, 2017). Here, CBZ
426 exposure resulted in the depletion of six amino acids at 24h (T24). As free amino acids are important
427 osmoregulators in mollusks, this decrease may alter osmotic homeostasis (Viant et al., 2003). In
428 addition, KEGG pathway "choline metabolism" was enriched. Choline is a precursor of betaine,
429 another osmoregulator (Ueland, 2011). As such, Ca^{2+} channels might be an early toxicity target of CBZ
430 in *D. polymorpha*, supporting a similar mode of action of CBZ than in vertebrates (Ambrósio et al.,
431 2002; von Borstel Smith et al., 2007; Fabbri and Franzellitti, 2016).

432 Besides, Ca^{2+} is an important secondary messenger (Liu et al., 2007; Puri, 2020), and CBZ
433 exposure at T24 caused the depletion of seven proteinogenic amino acids and the enrichment of
434 differential abundant proteins (DAPs) involved in protein turnover, *e.g.* "negative regulation of
435 protein ubiquitination". Similarly, in digestive glands of males of *M. galloprovincialis*, exposure to
436 0.08 and 8 µg L^{-1} 3d caused a higher abundance of proteins involved in RNA transcription and protein
437 translation (Dumas et al., 2022b). As such, CBZ appeared here to alter signal transduction, and
438 modulate protein abundance, most likely to cope with the pollutant.

439 Methylmercury (MeHg) exposure to a concentration representative of contaminated areas
440 resulted in the enrichment of the "epithelium development", "positive regulation of nematode larval
441 development" and "barbed-end actin filament capping", suggesting an alteration of cytoskeleton and
442 cellular development. MeHg was previously shown to cause an increase of DAPs involved in
443 cytoskeleton up to 55x in *Gammarus fossarum* exposed by diet to 20 µg L^{-1} MeHg 7d (Cosio et al.,
444 2021). As such, the cytoskeleton appeared as a toxicity target of MeHg in *D. polymorpha*, supporting

445 a similar mode of action than the one reported in vertebrates (Secor et al., 2011; Yadetie et al.,
446 2016). Although 55 DAPs were observed, no significant modulation appeared at the metabolome
447 level, suggesting that proteome modulations were sufficient to deal with MeHg in our experimental
448 conditions.

449 The co-exposure caused the specific enrichment of "dopaminergic synapse" and the depletion of
450 GABA at T24, suggesting neurotoxicity. GABA is an inhibitor neurotransmitter which can regulate
451 dopamine neurotransmission (Bak et al., 2006). In *Corbicula fluminea* 0.5 µg L^{-1} CBZ 30d modulated 3
452 genes coding for one GABA transporter and two GABA receptors in gonads, the mantle and digestive
453 glands (Chen et al., 2021). Hg is known to alter the regulation of GABA amount in vertebrates
454 (Fitsanakis and Aschner, 2005). GABA is involved in reproduction, notably steroidogenesis (Maguire
455 et al., 2005) and spermatogenesis in scallops (Watanabe et al., 2014; Nagasawa et al., 2015). In
456 *Mytilus edulis*, analyses along seasons showed that GABA was linked to the gonadal development
457 (Kronberg et al., 2021). Similarly, the co-exposure might cause reprotoxicity in *D. polymorpha*: 5 µg L^{-1}
458 CBZ 15 weeks delayed spermatogenesis (Magniez et al., 2018). Nonetheless, here no DAP was
459 involved in spermatogenesis. As such, data underlined the need for more studies targeting gonads.

460

461 4.2. Common molecular toxicity pathways

462 CBZ and MeHg single and co-exposures did not significantly modulate antioxidant system. MeHg
463 and the co-exposure increased 1.6x the abundance of GST2 at the proteome level at T24, without
464 significant modulation in GST enzyme activity level. This suggested ROS production, as expected for
465 MeHg and CBZ exposure, and that observed increase in protein abundance likely happened to
466 maintain cellular functions. In *Chlamys farreri* exposure to 50 ng L^{-1} IHg 96h decreased 1.2x CAT and
467 1.5x GPx activities in digestive glands but did not cause a lipid peroxidation (Zhang et al., 2010). In
468 the same line, in *Cerastoderma edule*, exposure to 5 µg L^{-1} CBZ 48h increased 2x the ROS production
469 (H_2O_2) without significant change in SOD, CAT and GST activities (Jaouani et al., 2022). In copepods

Tigriopus japonicus and *Paracyclina nana*, exposure to 1 – 1000 ng L^{-1} MeHg 24h increased 1.2 to 1.4x ROS levels and modulated the phosphorylation status of mitrogen activated protein kinase (MAPK) pathways (1.2 to 1.5x; Lee et al., 2017a, 2017b). Data globally supported an efficient basal level of antioxidant defenses in *D. polymorpha.* Unchanged antioxidant activities and LOOH abundance suggested that *D. polymorpha* tolerated our experimental conditions. In the same line, single and co-exposure unchanged mt gene expression level. In *Caenorhabditis elegans*, exposure to 60 mg L^{-1} MeHg 15h did not modulate mt gene expression, but a knockout mutant of mt-gene showed a higher sensitivity to MeHg (Helmcke and Aschner, 2010), supporting that background MT was instrumental for defense against MeHg. This could also be the case in *D. polymorpha*, here.

Single and co-exposures at T24 also caused a modulation of DAPs involved in protein turnover (*e.g.* transcription, translation) and amino acid metabolism, while CBZ at T24 and the co-exposure at both timepoints caused an alteration of proteinogenic amino acids. Similarly, in digestive glands of *M. galloprovincialis*, 80 ng L^{-1} and 8 µg L^{-1} CBZ 3d modulated proteins involved in amino acid metabolism and transcription/translation processes (Dumas et al., 2022b). Authors hypothesized an increase of protein biosynthesis due to a cellular stress (Dumas et al., 2022b). In adductor muscles of *Ruditapes philippinarum*, 20 µg L^{-1} IHg 48h caused a reduction of alanine, arginine, branched-chain amino acids, glutamine, glutamate, glycine compared to Ctl (Liu et al., 2011). Globally, data suggested here that both CBZ and MeHg increased transcription and translation, most likely to fight against potential toxicity resulting from their bioaccumulation.

In aquatic invertebrates, amino acid consumption can produce energy in response to stress through an alternative pathway (Sokolova et al., 2012). Here single and co-exposures altered energy metabolism through amino acid, lipid and sugar consumption. CBZ, MeHg and the co-exposure at T24 caused a modulation of DAPs involved in the energy metabolism (*e.g.* "glucose homeostasis", "glycerolipid metabolism"). In addition, the co-exposure resulted in a depletion of fumaric acid and glyceric acid at T24, and an accumulation of glycerolipids (glycerol, glycerol-3-phosphate) and lactic

acid at T72. Fumaric acid is an important metabolite of TCA cycle; glyceric acid is involved in glycerolipid metabolism; and lactic acid is an end product of anaerobic pyruvate metabolism of glucose (De Zwaan and Dando, 1984). In the same line, "HIF signaling pathway" was enriched by MeHg single exposure, although oxygen saturation was stable in all exposures. HIF is a transcription factor maintaining cellular homeostasis in aquatic invertebrates in suboxic conditions (Giannetto et al., 2015). Similarly, in gills of *Mytilus galloprovincialis* in a Hg-polluted site in the Mediterranean Sea, hif-α gene expression was up-regulated 2.3x in comparison with a reference site (Maisano et al., 2017). In astrocytes of rat, 2 mg L^{-1} MeHg 30 min down-regulated 2.2x the expression of hif-1α, together with a 1.5x decrease of cell proliferation (Chang et al., 2019). Here, shift from aerobic to anaerobic metabolism through HIF 1 signaling pathway in *D. polymorpha* most likely prevented cytotoxic effect of MeHg, that would have caused metabolome alteration that are not observed here. Thus, data here suggested a switch from TCA cycle to an anaerobic metabolism, particularly in the co-exposure. Similarly, in adductor muscles of *R. philippinarum*, exposure to 20 µg L^{-1} IHg 48h caused an accumulation of lactate and succinate, and a depletion of acetoacetate and ATP *vs* Ctl (Liu et al., 2011).

Data here supported that in *D. polymorpha* the co-exposure triggered more alterations than single exposures at concentrations representative of contaminated areas, although the zebra mussel appears to tolerate these experimental conditions. As bioaccumulation did not seem to be correlated to the number of molecular modulations, this is attributed to the combined molecular toxicity mechanisms of both pollutants. Similarly, in *D. polymorpha*, the co-exposure to 3.9 µg L^{-1} CBZ + 280 ng L^{-1} MeHg resulted in no significant modulation at T24 in single and the co-exposure, while 7d co-exposure caused a significant decrease of 25 metabolites involved in antioxidant, amino acid and energy metabolism (*e.g.* GSH metabolism, glycine, serine and threonine metabolism, galactose metabolism) (Baratange et al., 2022).

5. Conclusion

The present work combined several approaches at different biological organization levels to identify molecular toxicity pathways of CBZ and MeHg in *D. polymorpha* (figure 6). Alterations of amino acid metabolism, energy metabolism, development, and stress responses were common to the three exposures. In line with the initial hypothesis, the co-exposure caused more alterations than single exposures in *D. polymorpha*. Nonetheless, data showed a low-toxicity level, supporting that exposures were well tolerated by *D. polymorpha*. Untargeted proteogenomics identified proteins involved “calcium signaling pathway” for CBZ exposure, ”HIF-1”, and “Toll and Imd signaling pathways” for MeHg exposure and ”dopaminergic synapse” for the co-exposure. These specific responses underlined the challenge to predict effects of a co-exposure based on responses observed in single exposures. As such, it is a priority to consider pollutant cocktails in future research, particularly at environmental concentrations, to better understand and anticipate the ecotoxicity of pollutants in more complex and realistic scenarios.

Funding

This research was funded by Grand Reims through the Aquasurv Chair, by the French National program EC2CO (Ecosphere Continentale et Cotiere) through the CARMA n◦12837 program.

Declaration of competing interests

The authors have no competing interests to declare.

Acknowledgements

542 We are grateful to the Mobicyte Platform at URCA and EcoChimie Platform (EcoChim) at UMS OSUR
543 3343 for access to qPCR and metabolomics facilities, respectively and technical support. Authors
544 would like to thank Nicolas Borie and Fanny Louis for technical help, and Maxime Leprêtre for
545 analytical advice. Authors also benefited from the French GDR “Aquatic Ecotoxicology” framework
546 which aims at fostering stimulating scientific discussions and collaborations for more integrative
547 approaches.

548

549 **References**

550 Aguirre-Martínez, G.V., DelValls, T.A., Martín-Díaz, M.L., 2016. General stress, detoxification
551 pathways, neurotoxicity and genotoxicity evaluated in Ruditapes philippinarum exposed to
552 human pharmaceuticals. Ecotoxicol. Environ. Saf. 124, 18–31.
553 https://doi.org/10.1016/j.ecoenv.2015.09.031
554 Almeida, Â., Freitas, R., Calisto, V., Esteves, V.I., Schneider, R.J., Soares, A.M.V.M., Figueira, E., 2015.
555 Chronic toxicity of the antiepileptic carbamazepine on the clam Ruditapes philippinarum.
556 Comp. Biochem. Physiol. Part C Toxicol. Pharmacol. 172–173, 26–35.
557 https://doi.org/10.1016/j.cbpc.2015.04.004
558 Amachree, D., Moody, A.J., Handy, R.D., 2014. Comparison of intermittent and continuous exposures
559 to inorganic mercury in the mussel, Mytilus edulis: Accumulation and sub-lethal physiological
560 effects. Ecotoxicol. Environ. Saf. 109, 133–142.
561 https://doi.org/10.1016/j.ecoenv.2014.07.025
562 Ambrósio, A.F., Soares-da-Silva, P., Carvalho, C.M., Carvalho, A.P., 2002. Mechanisms of Action of
563 Carbamazepine and Its Derivatives, Oxcarbazepine, BIA 2-093, and BIA 2-024 10.
564 Andreu, V., Gimeno-García, E., Pascual, J.A., Vazquez-Roig, P., Picó, Y., 2016. Presence of
565 pharmaceuticals and heavy metals in the waters of a Mediterranean coastal wetland:
566 Potential interactions and the influence of the environment. Sci. Total Environ. 540, 278–286.
567 https://doi.org/10.1016/j.scitotenv.2015.08.007
568 Armengaud, J., Trapp, J., Pible, O., Geffard, O., Chaumot, A., Hartmann, E.M., 2014. Non-model
569 organisms, a species endangered by proteogenomics. J. Proteomics 105, 5–18.
570 https://doi.org/10.1016/j.jprot.2014.01.007
571 Baali, H., Cosio, C., 2022. Effects of carbamazepine in aquatic biota. Environmental Science: Processes
572 & Impacts, 2. https://doi.org/10.1039/D1EM00328C

573 Bak, L.K., Schousboe, A., Waagepetersen, H.S., 2006. The glutamate/GABA-glutamine cycle:
574 aspects of transport, neurotransmitter homeostasis and ammonia transfer. J.
575 Neurochem. 98, 641–653. https://doi.org/10.1111/j.1471-4159.2006.03913.x
576 Baratange, C., Paris-Palacios, S., Bonnard, I., Delahaut, L., Grandjean, D., Wortham, L., Sayen, S.,
577 Gallorini, A., Michel, J., Renault, D., Breider, F., Loizeau, J.-L., Cosio, C., 2022. Metabolic,
578 cellular and defense responses to single and co-exposure to carbamazepine and
579 methylmercury in Dreissena polymorpha. Environ Pollut. 300, 118933.
580 https://doi.org/10.1016/j.envpol.2022.118933
581 Binelli, A., Della Torre, C., Magni, S., Parolini, M., 2015. Does zebra mussel (Dreissena polymorpha)
582 represent the freshwater counterpart of Mytilus in ecotoxicological studies? A critical review.
583 Environ. Pollut. 196, 386–403. https://doi.org/10.1016/j.envpol.2014.10.023
584 Brandts, I., Teles, M., Gonçalves, A.P., Barreto, A., Franco-Martinez, L., Tvarijonaviciute, A., Martins,
585 M.A., Soares, A.M.V.M., Tort, L., Oliveira, M., 2018. Effects of nanoplastics on Mytilus
586 galloprovincialis after individual and combined exposure with carbamazepine. Sci. Total
587 Environ. 643, 775–784. https://doi.org/10.1016/j.scitotenv.2018.06.257
588 Brinke B., 2017. Toxicogenomics in environmental science. In vitro Environmental Toxicology –
589 Concepts, Application and Assessment, Reifferscheid et al, Eds Springer International
590 Publishing, 159.
591 Calisto, V., Bahlmann, A., Schneider, R.J., Esteves, V.I., 2011. Application of an ELISA to the
592 quantification of carbamazepine in ground, surface and wastewaters and validation with LC-
593 MS/MS. Chemosphere 84 (11): 1708-15.
594 https://doi.org/10.1016/j.chemosphere.2011.04.072
595 Carvalho, P.C., Yates, J.R., Barbosa, V.C., 2012. Improving the TFold test for differential shotgun
596 proteomics. Bioinformatics 28, 1652–1654. https://doi.org/10.1093/bioinformatics/bts247
597 Chang, J., Yang, B., Zhou, Y., Yin, C., Liu, T., Qian, H., Xing, G., Wang, S., Li, F., Zhang, Y., Chen, D.,
598 Aschner, M., Lu, R., 2019. Acute methylmercury exposure and the hypoxia-inducible factor-

599 1α signaling pathway under normoxic conditions in the rat brain and astrocytes *in vitro*.
600 Environmental Health Perspectives 127 (12), 127006. https://doi.org/10.1289/EHP5139
601 Chen, H., Zha, J., Liang, X., Li, J., Wang, Z., 2014. Effects of the human antiepileptic drug
602 carbamazepine on the behavior, biomarkers, and heat shock proteins in the Asian clam
603 Corbicula fluminea. Aquat. Toxicol. 155, 1–8. https://doi.org/10.1016/j.aquatox.2014.06.001
604 Chen, H., Gu, X., Zeng, Q., Mao, Z., Martyniuk, C.J., 2021. Characterization of the GABAergic system in
605 Asian clam Corbicula fluminea: Phylogenetic analysis, tissue distribution, and response to the
606 aquatic contaminant carbamazepine. Comp. Biochem. Physiol. Part C Toxicol. Pharmacol.
607 239, 108896. https://doi.org/10.1016/j.cbpc.2020.108896
608 Christie-Oleza, J.A., Fernandez, B., Nogales, B., Bosch, R., Armengaud, J., 2012. Proteomic insights
609 into the lifestyle of an environmentally relevant marine bacterium. ISME J. 6, 124–135.
610 https://doi.org/10.1038/ismej.2011.86
611 Clara, M., Strenn, B., Kreuzinger, N., 2004. Carbamazepine as a possible anthropogenic marker in the
612 aquatic environment: investigations on the behaviour of Carbamazepine in wastewater
613 treatment and during groundwater infiltration. Water Res. 38, 947–954.
614 https://doi.org/10.1016/j.watres.2003.10.058
615 Contardo-Jara, V., Lorenz, C., Pflugmacher, S., Nützmann, G., Kloas, W., Wiegand, C., 2011. Exposure
616 to human pharmaceuticals Carbamazepine, Ibuprofen and Bezafibrate causes molecular
617 effects in Dreissena polymorpha. Aquat. Toxicol. 105, 428–437.
618 https://doi.org/10.1016/j.aquatox.2011.07.017
619 Coppola, F., Almeida, Â., Henriques, B., Soares, A.M.V.M., Figueira, E., Pereira, E., Freitas, R., 2017.
620 Biochemical impacts of Hg in Mytilus galloprovincialis under present and predicted warming
621 scenarios. Sci. Total Environ. 601–602, 1129–1138.
622 https://doi.org/10.1016/j.scitotenv.2017.05.201
623 Cosio, C., Degli-Esposti, D., Almunia, C., Gaillet, V., Sartelet, H., Armengaud, J., Chaumot, A., Geffard,
624 O., Geffard, A., 2021. Subcellular Distribution of Dietary Methyl-Mercury in *Gammarus*

fossarum and Its Impact on the Amphipod Proteome. Environ. Sci. Technol. 55, 10514–10523. https://doi.org/10.1021/acs.est.1c02385

D'Aniello, A., 2007. d-Aspartic acid: An endogenous amino acid with an important neuroendocrine role. Brain Res. Rev. 53, 215–234. https://doi.org/10.1016/j.brainresrev.2006.08.005

De Zwaan, A., Dando, P., 1984. Phosphoenolpyruvate metabolism in bivalve molluscs. Mol. Physiol. 5, 285-310

Dumas, T., Courant, F., Fenet, H., Gomez, E., 2022a. Environmental Metabolomics Promises and Achievements in the Field of Aquatic Ecotoxicology: Viewed through the Pharmaceutical Lens. Metabolites 12, 186. https://doi.org/10.3390/metabo12020186

Dumas, T., Courant, F., Almunia, C., Boccard, J., Rosain, D., Duporté, G., Armengaud, J., Fenet, H., Gomez, E., 2022b. An integrated metabolomics and proteogenomics approach reveals molecular alterations following carbamazepine exposure in the male mussel Mytilus galloprovincialis. Chemosphere 286, 131793. https://doi.org/10.1016/j.chemosphere.2021.131793

Dvory, N. Z., Livshitz, Y., Kuznetsov, M., Adar, E., Gasser, G., Pankratov, I., Lev, O., Yakirevich, A., 2018. Caffeine vs. carbamazepine as indicators of wastewater pollution in a karst aquifer, Hydrol. Earth Syst. Sci., 22, 6371–6381, https://doi.org/10.5194/hess-22-6371-2018

ETOX, 2011. "Datenbank für ökotoxikologische Wirkungsdaten und Qualitätsziele." from http://webetox.uba.de/webETOX/index.do (12/10/2021)

Fabbri, E., Franzellitti, S., 2016. Human pharmaceuticals in the marine environment: Focus on exposure and biological effects in animal species: Fate and effects of pharmaceuticals in marine environments. Environ. Toxicol. Chem. 35, 799–812. https://doi.org/10.1002/etc.3131

Fang, Y., Yang, H., Liu, B., 2012. Tissue-specific response of metallothionein and superoxide dismutase in the clam Mactra veneriformis under sublethal mercury exposure. Ecotoxicology 21, 1593–1602. https://doi.org/10.1007/s10646-012-0938-8

651 Fitsanakis, V.A., Aschner, M., 2005. The importance of glutamate, glycine, and γ-aminobutyric acid
652 transport and regulation in manganese, mercury and lead neurotoxicity. Toxicology and
653 applied pharmacology 204, 3, 343-354. https://doi.org/10.1016/j.taap.2004.11.013
654 Giannetto, A., Maisano, M., Cappello, T., Oliva, S., Parrino, V., Natalotto, A., De Marco, G., Barberi, C.,
655 Romeo, O., Mauceri, A., Fasulo, S, 2015. Hypoxia-Inducible Factor α and Hif-prolyl
656 Hydroxylase Characterization and Gene Expression in Short-Time Air-Exposed Mytilus
657 galloprovincialis. Mar. Biotechnol. (NY) 17(6):768-81. doi: 10.1007/s10126-015-9655-7.
658 Gonzalez, P., Pierron, F., 2015. Omics in Aquatic Ecotoxicology, in: Aquatic Ecotoxicology. Elsevier, pp.
659 183–203. https://doi.org/10.1016/B978-0-12-800949-9.00008-5
660 González-Mira, A., Varó, I., Solé, M., Torreblanca, A., 2016. Drugs of environmental concern modify
661 Solea senegalensis physiology and biochemistry in a temperature-dependent manner.
662 Environ. Sci. Pollut. Res. 23, 20937–20951. https://doi.org/10.1007/s11356-016-7293-x
663 González-Mira, A., Torreblanca, A., Hontoria, F., Navarro, J.C., Mañanós, E., Varó, I., 2018. Effects of
664 ibuprofen and carbamazepine on the ion transport system and fatty acid metabolism of
665 temperature conditioned juveniles of Solea senegalensis. Ecotoxicol. Environ. Saf. 148, 693–
666 701. https://doi.org/10.1016/j.ecoenv.2017.11.023
667 Gouveia, D., Almunia, C., Cogne, Y., Pible, O., Degli-Esposti, D., Salvador, A., Cristobal, S., Sheehan, D.,
668 Chaumot, A., Geffard, O., Armengaud, J., 2019. Ecotoxicoproteomics: A decade of progress in
669 our understanding of anthropogenic impact on the environment. J. Proteomics 198, 66–77.
670 https://doi.org/10.1016/j.jprot.2018.12.001
671 Han, M., Zhang, C., Suglo, P., Sun, S., Wang, M., Su, T., 2021. l-Aspartate: An Essential Metabolite for
672 Plant Growth and Stress Acclimation. Molecules 26, 1887.
673 https://doi.org/10.3390/molecules26071887
674 Hani, Y.M.I., Prud'Homme, S.M., Nuzillard, J.-M., Bonnard, I., Robert, C., Nott, K., Ronkart, S.,
675 Dedourge-Geffard, O., Geffard, A., 2021. 1H-NMR metabolomics profiling of zebra mussel

(Dreissena polymorpha): A field-scale monitoring tool in ecotoxicological studies. Environ. Pollut. 270, 116048. https://doi.org/10.1016/j.envpol.2020.116048

Hartmann, E.M., Allain, F., Gaillard, JC., Pible, O., Armengaud, J., 2014. Taking the Shortcut for High-Throughput Shotgun Proteomic Analysis of Bacteria. In: Vergunst A., O'Callaghan D. (eds) Host-Bacteria Interactions. Methods in Molecular Biology (Methods and Protocols), vol 1197. Humana Press, New York, NY. https://doi.org/10.1007/978-1-4939-1261-2_16

Heberle, H., Meirelles, G.V., da Silva, F.R., Telles, G.P., Minghim, R., 2015. InteractiVenn: a web-based tool for the analysis of sets through Venn diagrams. BMC Bioinformatics 16, 169. https://doi.org/10.1186/s12859-015-0611-3

Helmcke, K.J., Aschner, M., 2010. Hormetic effect of methylmercury on Caenorhabditis elegans. Toxicol. Appl. Pharmacol. 248, 156–164. https://doi.org/10.1016/j.taap.2010.07.023

Jaouani, R., Dellali, M., Mouneyrac, C., Hassine, S.B., Ali, M.B., Hedfi, A., Hassan, M.M., Beyrem, H., Boufahja, F., 2022. Assessment of carbamazepine acute toxicity in the cockle Cerastoderma edule through chemical, physiological and biochemical tools. Braz. J. Biol. 82, e247035. https://doi.org/10.1590/1519-6984.247035

Ji, C., Wu, H., Wei, L., Zhao, J., Yu, J., 2013. Proteomic and metabolomic analysis reveal gender-specific responses of mussel Mytilus galloprovincialis to 2,2′,4,4′-tetrabromodiphenyl ether (BDE 47). Aquat. Toxicol. 140–141, 449–457. https://doi.org/10.1016/j.aquatox.2013.07.009

Ji, C., Zhao, J., Wu, H., 2014b. Gender-specific metabolic responses in gonad of mussel Mytilus galloprovincialis to 2,2′,4,4′-tetrabromodiphenyl ether. Environ. Toxicol. Pharmacol. 37, 1116–1122. https://doi.org/10.1016/j.etap.2014.04.007

Jiang, W., Fang, Jianguang, Gao, Y., Du, M., Fang, Jinghui, Wang, X., Li, F., Lin, F., Jiang, Z., 2019. Biomarkers responses in Manila clam, Ruditapes philippinarum after single and combined exposure to mercury and benzo[a]pyrene. Comp. Biochem. Physiol. Part C Toxicol. Pharmacol. 220, 1–8. https://doi.org/10.1016/j.cbpc.2019.02.010

Kase R. 2010. Stoffdatenblattentwurf für Carbamazepin (Stand 15/02/2010; update 30/04/2010).

Kerambrun, E., Rioult, D., Delahaut, L., Evariste, L., Pain-Devin, S., Auffret, M., Geffard, A., David, E., 2016. Variations in gene expression levels in four European zebra mussel, Dreissena polymorpha, populations in relation to metal bioaccumulation: A field study. Ecotoxicol. Environ. Saf. 134, 53–63. https://doi.org/10.1016/j.ecoenv.2016.08.018

Kershaw, J.L., Hall, A.J., 2019. Mercury in cetaceans: Exposure, bioaccumulation and toxicity. Sci. Total Environ. 694, 133683. https://doi.org/10.1016/j.scitotenv.2019.133683

Klein, G., Mathé, C., Biola-Clier, M., Devineau, S., Drouineau, E., Hatem, E., Marichal, L., Alonso, B., Gaillard, J.-C., Lagniel, G., Armengaud, J., Carrière, M., Chédin, S., Boulard, Y., Pin, S., Renault, J.-P., Aude, J.-C., Labarre, J., 2016. RNA-binding proteins are a major target of silica nanoparticles in cell extracts. Nanotoxicology 10, 1555–1564. https://doi.org/10.1080/17435390.2016.1244299

Klimova, Y.S., Chuiko, G.M., Gapeeva, M.V., Pesnya, D.S., 2017. The use of biomarkers of oxidative stress in zebra mussel Dreissena polymorpha (Pallas, 1771) for chronic anthropogenic pollution assessment of the Rybinsk Reservoir. Contemp. Probl. Ecol. 10, 178–183. https://doi.org/10.1134/S199542551702007X

Kronberg, J., Byrne, J.J., Jansen, J., Antczak, P., Hines, A., Bignell, J., Katsiadaki, I., Viant, M.R., Falciani, F., 2021. Modeling the metabolic profile of Mytilus edulis reveals molecular signatures linked to gonadal development, sex and environmental site. Sci. Rep. 11, 12882. https://doi.org/10.1038/s41598-021-90494-y

Lee, Y.H., Kang, H.-M., Kim, D.-H., Wang, M., Jeong, C.-B., Lee, J.-S., 2017a. Adverse effects of methylmercury (MeHg) on life parameters, antioxidant systems, and MAPK signaling pathways in the copepod Tigriopus japonicus. Aquat. Toxicol. 184, 133–141. https://doi.org/10.1016/j.aquatox.2017.01.010

Lee, Y.H., Kim, D.-H., Kang, H.-M., Wang, M., Jeong, C.-B., Lee, J.-S., 2017b. Adverse effects of methylmercury (MeHg) on life parameters, antioxidant systems, and MAPK signaling

pathways in the rotifer Brachionus koreanus and the copepod Paracyclopina nana. Aquat. Toxicol. 190, 181–189. https://doi.org/10.1016/j.aquatox.2017.07.006

Liu, X., Zhang, L., You, L., Cong, M., Zhao, J., Wu, H., Li, C., Liu, D., Yu, J., 2011. Toxicological responses to acute mercury exposure for three species of Manila clam Ruditapes philippinarum by NMR-based metabolomics. Environ. Toxicol. Pharmacol. 31, 323–332. https://doi.org/10.1016/j.etap.2010.12.003

Liu, Z.-M., Chen, G.G., Vlantis, A.C., Tse, G.M., Shum, C.K.Y., van Hasselt, C.A., 2007. Calcium-mediated activation of PI3K and p53 leads to apoptosis in thyroid carcinoma cells. Cell. Mol. Life Sci. 64, 1428–1436. https://doi.org/10.1007/s00018-007-7107-x

López-Pedrouso, M., Varela, Z., Franco, D., Fernández, J.A., Aboal, J.R., 2020. Can proteomics contribute to biomonitoring of aquatic pollution? A critical review. Environ. Pollut. 267, 115473. https://doi.org/10.1016/j.envpol.2020.115473

Louis, F., Devin, S., Giambérini, L., Potet, M., David, E., Pain-Devin, S., 2019. Energy allocation in two dreissenid species under metal stress. Environ. Pollut. 245, 889–897. https://doi.org/10.1016/j.envpol.2018.11.079

Louis, F., Rocher, B., Barjhoux, I., Bultelle, F., Dedourge-Geffard, O., Gaillet, V., Bonnard, I., Delahaut, L., Pain-Devin, S., Geffard, A., Paris-Palacios, S., David, E., 2020. Seasonal monitoring of cellular energy metabolism in a sentinel species, Dreissena polymorpha (bivalve): Effect of global change? Sci. Total Environ. 725, 138450. https://doi.org/10.1016/j.scitotenv.2020.138450

Magniez, G., Franco, A., Geffard, A., Rioult, D., Bonnard, I., Delahaut, L., Joachim, S., Daniele, G., Vulliet, E., Porcher, J.-M., Bonnard, M., 2018. Determination of a new index of sexual maturity (ISM) in zebra mussel using flow cytometry: interest in ecotoxicology. Environ. Sci. Pollut. Res. 25, 11252–11263. https://doi.org/10.1007/s11356-017-9256-2

751 Maguire, J.L., Stell, B.M., Rafizadeh, M., Mody, I., 2005. Ovarian cycle-linked changes in GABA(A)
752 receptors mediating tonic inhibition alter seizure susceptibility and anxiety. Nat. Neurosci. 8,
753 797–804.
754 Mahat, N.A., Muktar, N.K., Ismail, R., Abdul Razak, F.I., Abdul Wahab, R., Abdul Keyon, A.S., 2018.
755 Toxic metals in Perna viridis mussel and surface seawater in Pasir Gudang coastal area,
756 Malaysia, and its health implications. Environ. Sci. Pollut. Res. 25, 30224–30235.
757 https://doi.org/10.1007/s11356-018-3033-8
758 Maisano, M., Cappello, T., Natalotto, A., Vitale, V., Parrino, V., Giannetto, A., Oliva, S., Mancini, G.,
759 Cappello, S., Mauceri, A., Fasulo, S., 2017. Effects of petrochemical contamination on caged
760 marine mussels using a multi-biomarker approach: Histological changes, neurotoxicity and
761 hypoxic stress. Mar. Environ. Res. 128, 114–123.
762 https://doi.org/10.1016/j.marenvres.2016.03.008
763 Metian, M., Pouil, S., Dupuy, C., Teyssié, J.-L., Warnau, M., Bustamante, P., 2020. Influence of food
764 (ciliate and phytoplankton) on the trophic transfer of inorganic and methyl-mercury in the
765 Pacific cupped oyster Crassostrea gigas. Environ. Pollut. 257, 113503.
766 https://doi.org/10.1016/j.envpol.2019.113503
767 Minamata International Convention, 2013. https://www.mercuryconvention.org/en
768 Morosetti, B., Freitas, R., Pereira, E., Hamza, H., Andrade, M., Coppola, F., Maggioni, D., Della Torre,
769 C., 2020. Will temperature rise change the biochemical alterations induced in Mytilus
770 galloprovincialis by cerium oxide nanoparticles and mercury? Environ. Res. 188, 109778.
771 https://doi.org/10.1016/j.envres.2020.109778
772 Nagasawa, K., Oouchi, H., Itoh, N., Takahashi, K.G., Osada, M., 2015. In vivo administration of scallop
773 GnRH-like peptide influences on gonad development in the yesso scallop, Patinopectein
774 yessoensis. PLoS ONE 10, 6. https://doi.org/10.1371/journal.pone.0129571

775 Oldenkamp, R., Beusen, A.H.W., Huijbregts, M.A.J., 2019. Aquatic risks from human
776 pharmaceuticals—modelling temporal trends of carbamazepine and ciprofloxacin at the
777 global scale. Environ. Res. Lett. 14, 034003. https://doi.org/10.1088/1748-9326/ab0071
778 Oliveira, P., Almeida, Â., Calisto, V., Esteves, V.I., Schneider, R.J., Wrona, F.J., Soares, A.M.V.M.,
779 Figueira, E., Freitas, R., 2017. Physiological and biochemical alterations induced in the mussel
780 Mytilus galloprovincialis after short and long-term exposure to carbamazepine. Water Res.
781 117, 102–114. https://doi.org/10.1016/j.watres.2017.03.052
782 Paul-Pont, I., Gonzalez, P., Montero, N., de Montaudouin, X., Baudrimont, M., 2012. Cloning,
783 characterization and gene expression of a metallothionein isoform in the edible cockle
784 Cerastoderma edule after cadmium or mercury exposure. Ecotoxicol. Environ. Saf. 75, 119–
785 126. https://doi.org/10.1016/j.ecoenv.2011.08.025
786 Pierozan, P., Biasibetti, H., Schmitz, F., Avila, H., Gonçalves Fernandes, C., Pessoa-Pureur, R., Wyse,
787 A.T.S., 2017. Neurotoxicity of methylmercury in isolated astrocytes and neurons: the
788 cytoskeleton as a main target. Mol Neurobiol 54, 5752-5767.
789 https://doi.org/10.1007/s12035-016-0101-2
790 Puri, B.K., 2020. Calcium Signaling and Gene Expression. In: Islam M. (eds) Calcium Signaling.
791 Advances in Experimental Medicine and Biology, vol 1131. Springer, Cham.
792 https://doi.org/10.1007/978-3-030-12457-1_22
793 Pytharopoulou, S., Kournoutou, G.G., Leotsinidis, M., Georgiou, C.D., Kalpaxis, D.L., 2013.
794 Dysfunctions of the translational machinery in digestive gland of mussels exposed to mercury
795 ions. Aquat. Toxicol. 134–135, 23–33. https://doi.org/10.1016/j.aquatox.2013.02.014
796 Schmittgen, T.D., Livak, K.J., 2008. Analyzing real-time PCR data by the comparative CT method. Nat.
797 Protoc. 3, 1101–1108. https://doi.org/10.1038/nprot.2008.73
798 Seifter, J.L., Chang, H.-Y., 2017. Extracellular Acid-Base Balance and Ion Transport Between Body Fluid
799 Compartments. Physiology 32, 367–379. https://doi.org/10.1152/physiol.00007.2017

800 Sokolova, I.M., Frederich, M., Bagwe, R., Lannig, G., Sukhotin, A.A., 2012. Energy homeostasis as an
801 integrative tool for assessing limits of environmental stress tolerance in aquatic
802 invertebrates. Mar. Environ. Res. 79, 1–15. https://doi.org/10.1016/j.marenvres.2012.04.003
803 Sturn, A., Quackenbush, J., Trajanoski, Z., 2002. Genesis: cluster analysis of microarray data.
804 *Bioinformatics* 18(1):207-8. https://doi.org/10.1093/bioinformatics/18.1.207
805 Thiébaut, G., Tarayre, M., Jambon, O., Le Bris, N., Colinet, H., Renault, D., 2021. Variation of thermal
806 plasticity for functional traits between populations of an invasive aquatic plant from two
807 climatic regions. Hydrobiologia 848, 2077–2091. https://doi.org/10.1007/s10750-020-04452-
808 2
809 Thompson, J.A.J., Cosson, R.P., 1984. An improved electrochemical method for the quantification of
810 metallothioneins in marine organisms. Marine Env. Research 11-2, 137-152.
811 https://doi.org/10.1016/0141-1136(84)90027-8.
812 Todgham, A.E., Stillman, J.H., 2013. Physiological Responses to Shifts in Multiple Environmental
813 Stressors: Relevance in a Changing World. Integr. Comp. Biol. 53, 539–544.
814 https://doi.org/10.1093/icb/ict086
815 Ueland, P.M., 2011. Choline and betaine in health and disease. J. Inherit. Metab. Dis. 34: 3-15.
816 https://doi.org/10.1007/s10545-010-9088-4
817 Velez, C., Freitas, R., Antunes, S.C., Soares, A.M.V.M., Figueira, E., 2016. Clams sensitivity towards As
818 and Hg: A comprehensive assessment of native and exotic species. Ecotoxicol. Environ. Saf.
819 125, 43–54. https://doi.org/10.1016/j.ecoenv.2015.11.030
820 Verlicchi, P., Al Aukidy, M., Zambello, E., 2012. Occurrence of pharmaceutical compounds in urban
821 wastewater: Removal, mass load and environmental risk after a secondary treatment—A
822 review. Sci. Total Environ. 429, 123–155. https://doi.org/10.1016/j.scitotenv.2012.04.028
823 Viant, M.R., Rosenblum, E.S., Tjeerdema, R.S., 2003. NMR-Based Metabolomics: a powerful approach
824 for characterizing the effects of environmental stressors on organism health. Environ. Sci.
825 Technol. 37, 4982–4989. https://doi.org/10.1021/es034281x

826 von Borstel Smith, M., Crofoot, K., Rodriguez-Proteau, R., Filtz, T.M., 2007. Effects of phenytoin and
827 carbamazepine on calcium transport in Caco-2 cells. Toxicol. In Vitro 21, 855–862.
828 https://doi.org/10.1016/j.tiv.2007.02.008
829 Watanabe, M., Fukuda, A., Nabekura, J., 2014. The role of GABA in the regulation of GnRH neuros.
830 Frontiers in Neuroscience 8. https://doi.org/10.3389/fnins.2014.00387
831 Yadetie, F., Bjørneklett, S., Garberg, H.K., Oveland, E., Berven, F., Goksøyr, A., Karlsen, O.A., 2016.
832 Quantitative analyses of the hepatic proteome of methylmercury-exposed Atlantic cod
833 (Gadus morhua) suggest oxidative stress-mediated effects on cellular energy metabolism.
834 BMC Genomics 17, 554. https://doi.org/10.1186/s12864-016-2864-2
835 Zhang, Q.-H., Huang, L., Zhang, Y., Ke, C.-H., Huang, H.-Q., 2013. Proteomic approach for identifying
836 gonads differential proteins in the oyster (Crassostrea angulata) following food-chain
837 contamination with HgCl2. J. Proteomics 94, 37–53.
838 https://doi.org/10.1016/j.jprot.2013.08.018
839 Zhang, M., Shi, Y., Lu, Y., Johnson, A.C., Sarvajayakesavalu, S., Liu, Z., Su, C., Zhang, Y., Juergens, M.D.,
840 Jin, X., 2017. The relative risk and its distribution of endocrine disrupting chemicals,
841 pharmaceuticals and personal care products to freshwater organisms in the Bohai Rim,
842 China. Science of the Tot. Env. 590-591, 633-642.
843 http://dx.doi.org/10.1016/j.scitotenv.2017.03.011
844 Zhang, Y., Geißen, S.-U., Gal, C., 2008. Carbamazepine and diclofenac: Removal in wastewater
845 treatment plants and occurrence in water bodies. Chemosphere 73, 1151–1161.
846 https://doi.org/10.1016/j.chemosphere.2008.07.086
847 Zhang, Y., Song, J., Yuan, H., Xu, Y., He, Z., Duan, L., 2010. Biomarker responses in the bivalve
848 (Chlamys farreri) to exposure of the environmentally relevant concentrations of lead,
849 mercury, copper. Environ. Toxicol. Pharmacol. 30, 19–25.
850 https://doi.org/10.1016/j.etap.2010.03.008

851 Zhou, S., Kang, R., Ji, C., Kaufmann, H., 2018. Heavy metal distribution, contamination and analysis of
852 sources - Intertidal zones of Sandu Bay, Ningde, China. Mar. Pollut. Bull. 135, 1138–1144.
853 https://doi.org/10.1016/j.marpolbul.2018.08.056
854

855 **Table 1**: List of the ten most increased and reduced proteins (log_2 fold change *vs* Ctl; blastp,
856 Swissprot) in *D. polymorpha* exposed to CBZ (6.1 ± 0.2 µg L^{-1}), MeHg (460 ± 20 ng L^{-1}) and the co-
857 exposure at T24. Significant differences *vs* Ctl appear in bold.

Functional annotation	%sequence identity	E-value	CBZ	MeHg	CBZ + MeHg
Intracellular transport					
Importin-5	66.8%	< $1E^{-199}$	1.08	0.94	**1.45**
Protein transport protein Sec31A	59.5%	< $1E^{-199}$	0.77	**1.26**	**1.20**
Response to stress					
Calumenin-A-like	62.7%	$9.3E^{-139}$	0.68	1.14	**1.58**
Cathepsin L1-like	45.2%	$2.0E^{-40}$	0.26	0.68	**1.49**
Cathepsin L1 isoform X4	46.4%	$1.1E^{-75}$	**1.09**	**1.05**	**1.38**
CD109 antigen-like	46.6%	$2.8E^{-37}$	1.21	**1.58**	1.16
Cyclin-related protein FAM58A	56.1%	$1.4E^{-102}$	**-1.14**	-0.65	**-1.14**
Signal transduction					
Guanine nucleotide-binding protein G(S) subunit alpha	84%	< $1E^{-199}$	1.00	1.22	**1.42**
Phosphotransferase 2.7.1	48.2%	$3.9E^{-31}$	0.49	**1.49**	0.85
Receptor protein-tyrosine kinase	35.2%	$2.1E^{-16}$	**1.12**	0.42	0.00
Transcription and translation					
Alanine--glyoxylate aminotransferase	65.4%	$4.2E^{-180}$	0.00	0.74	**1.58**
Cleavage and polyadenylation specificity factor subunit 2	65.9%	< $1E^{-199}$	**1.32**	0.42	1.00
Eukaryotic translation initiation factor 3 subunit J	57.5%	$2.4E^{-84}$	**1.12**	1.00	**1.42**

Isoleucyl tRNA synthetase	48.2%	$1.7E^{-104}$	1.14	**1.68**	0.68
Pre-mRNA-splicing factor 3	63.9%	$< 1E^{-199}$	**1.68**	0.85	0.85
RNA-binding protein 4	67.2%	$2.1E^{-114}$	**1.22**	0.74	**1.15**
SAP domain-containing protein	43.0%	$7.1E^{-43}$	0.64	0.00	**1.47**
THO complex subunit 1	54.6%	$< 1E^{-199}$	1.00	**1.32**	**1.50**
tRNA nucleotidyltransferase (CCA-adding enzyme)	56.6%	$7.3E^{-165}$	0.70	**1.39**	**1.25**
Zinc finger ZZ-type and EF-hand domain-containing protein 1	56.7%	$< 1E^{-199}$	**1.14**	0.85	**1.38**
Others					
3-hydroxyisobutyrate dehydrogenase	35.9%	$6.9E^{+00}$	**-1.51**	**-1.74**	-0.74
Multifunctional fusion protein	65.5%	$7.1E^{-114}$	1.26	0.68	**1.68**
Por_secre_tail domain-containing protein	42.6%	$< 1E^{-199}$	**1.38**	0.93	1.20
Spectrin beta chain, non-erythrocytic 5	65.0%	$< 1E^{-199}$	**1.35**	**1.30**	1.06
Glutamate carboxypeptidase 2	48.4%	$< 1E^{-199}$	**1.14**	0.49	0.00
Uncharacterized					
Uncharacterized protein LOC116288423	40.0%	$4.4E^{-04}$	1.00	**1.86**	-0.68
Uncharacterized protein LOC116288423	41.5%	$1.1E^{-04}$	0.42	**1.81**	-0.26

858

859

860 **Table 2**: Relative gene expression levels of cat, gst, sod and mt genes, enzyme activities of CAT (U mg
861 prot^{-1}), GST (µmol CDNB g prot^{-1} min^{-1}), SOD (U mg prot^{-1}), abundance of MT (mg g prot^{-1}) and LOOH
862 (µmol TBH g prot^{-1}) in gonads, digestive glands, and gills of *D. polymorpha* exposed to CBZ (6.1 ± 0.2
863 µg L^{-1}), MeHg (460 ± 20 ng L^{-1}), the co-exposure, and Ctl at T24 and T72 (mean±SEM, n = 3 to 8).

	Ctl		CBZ		MeHg		CBZ+MeHg	
	T24	T72	T24	T72	T24	T72	T24	T72
GONADS								
cat	1.00±0.23	1.00±0.32	0.65±0.14	0.65±0.15	0.56±0.12	0.77±0.18	0.57±0.13	1.20±0.21
gst	1.00±0.32	1.00±0.23	1.10±0.12	0.77±0.08	0.71±0.18	0.56±0.09	0.43±0.14	0.81±0.14
sod	1.00±0.12	1.00±0.17	0.66±0.18	1.14±0.15	0.53±0.15	0.85±0.19	0.49±0.10	1.03±0.21
mt	1.00±0.18	1.00±0.32	0.86±0.25	0.78±0.15	0.61±0.18	0.81±0.16	0.43±0.10	0.81±0.30
CAT	55.5±3.3	52.9±5.1	50.2±6.2	60.5±5.4	59.3±5.0	50.8±3.2	72.5±2.8	51.1±5.1
GST	115±8	168±10	135±18	173±15	124±8	190±23	140±20	138±25
SOD	4.10±0.31	2.89±0.53	3.58±0.32	2.90±0.40	3.78±0.17	2.66±0.70	3.78±0.14	2.57±0.58
MT	9.07±0.21	8.73±0.24	10.6±0.8	10.5±0.7	10.1±0.4	8.97±0.35	10.5±0.4	7.50±0.34
LOOH	40.6±4.6	26.7±2.1	43.2±6.0	28.7±2.0	44.6±2.4	26.7±1.8	36.5±3.3	31.8±2.4
DIGESTIVE GLANDS								
cat	1.00±0.17	1.00±0.19	0.73±0.10	1.31±0.12	0.77±0.07	1.31±0.18	0.71±0.08	1.26±0.22
gst	1.00±0.22	1.00±0.22	0.72±0.14	1.44±0.34	0.75±0.17	1.08±0.32	0.70±0.10	1.50±0.31
sod	1.00±0.12	1.00±0.26	0.54±0.15	1.11±0.18	0.84±0.17	1.35±0.25	0.87±0.10	0.95±0.19
mt	1.00±0.17	1.00±0.40	0.93±0.18	1.09±0.32	0.92±0.26	1.25±0.12	0.86±0.18	0.78±0.17
CAT	130±10	160±9	127±10	173±11	130±7	149±8	113±15	204±25
GST	185±15	178±13	195±19	179±25	207±28	192±14	178±36	213±28
SOD	2.39±0.11	2.39±0.17	2.40±0.14	2.45±0.10	2.62±0.14	2.26±0.15	2.55±0.22	2.89±0.13
MT	16.4±0.8	15.4±0.3	17.2±0.5	15.9±0.5	16.8±0.3	15.3±0.9	19.6±0.5	18.1±0.6

LOOH	55.6±8.0	42.5±3.5	48.7±3.3	43.4±2.0	52.8±4.6	57.6±7.4	54.1±4.8	52.7±7.1
GILLS								
cat	1.00±0.12	1.00±0.22	1.27±0.26	1.52±0.26	0.86±0.18	1.14±0.11	1.68±0.24	1.15±0.13
gst	1.00±0.14	1.00±0.07	0.99±0.07	0.74±0.09	0.97±0.05	1.54±0.29	1.21±0.14	1.17±0.16
sod	1.00±0.11	1.00±0.23	1.33±0.16	1.32±0.31	0.90±0.14	1.23±0.57	1.67±0.22	1.57±0.39
mt	1.00±0.09	1.00±0.29	1.04±0.26	0.86±0.12	0.60±0.12	1.28±0.27	0.95±0.27	1.01±0.23
CAT	23.3±0.9	23.1±1.7	25.6±1.7	24.0±2.2	25.9±1.2	22.9±1.5	24.0±1.2	26.0±2.5
GST	130±11	105±4	106±9	106±11	139±6	109±8	128±9	112±8
SOD	2.34±0.05	2.40±0.11	2.34±0.16	2.21±0.15	2.50±0.10	2.12±0.06	2.21±0.06	2.30±0.09
MT	13.3±1.4	16.5±0.6	12.0±0.5	13.4±0.5	15.5±1.4	13.4±0.5	17.0±2.3	14.9±0.9
LOOH	28.9±4.0	31.2±5.6	40.9±5.6	27.5±5.0	34.1±5.3	33.7±2.3	27.8±3.6	29.8±3.3

866

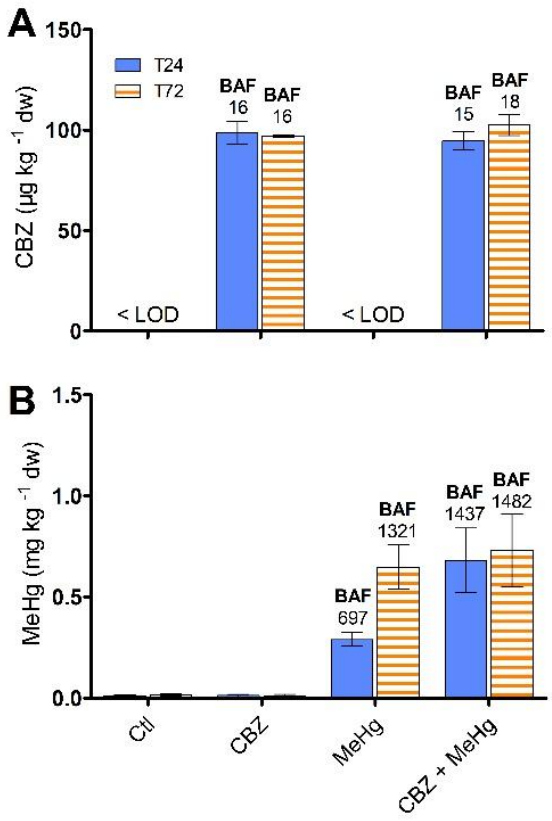

867

868

869 **Figure 1**: Bioaccumulation (mean ± SEM, n = 3) of (**A**) CBZ and (**B**) MeHg in *D. polymorpha* exposed to

870 CBZ (6.1 ± 0.2 µg L^{-1}), MeHg (460 ± 20 ng L^{-1}), the co-exposure (CBZ+MeHg) and Ctl. BAF (L kg^{-1}):

871 bioaccumulation factor

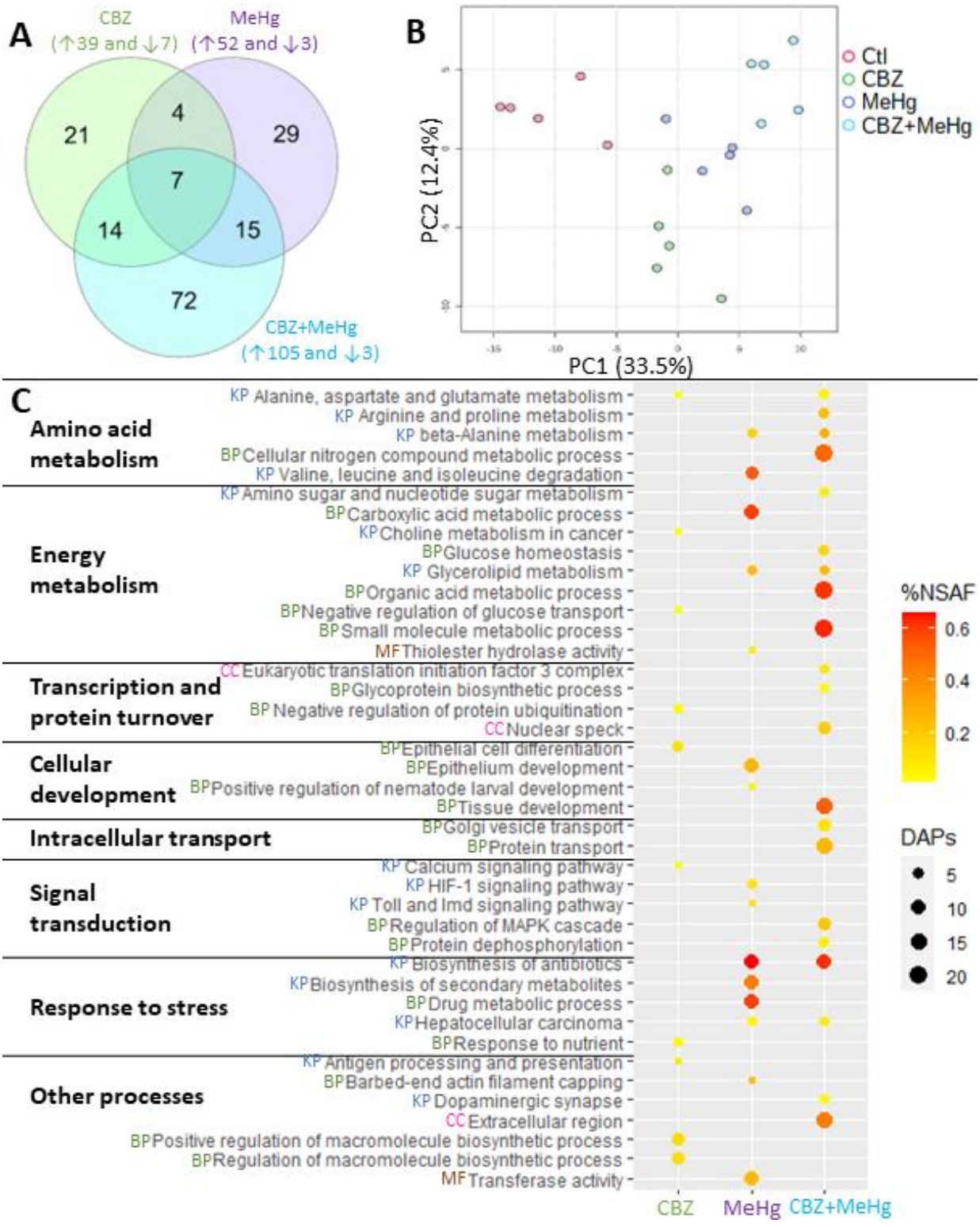

872

873 **Figure 2**: (**A**) Venn diagram of differentially abundant proteins, (**B**) PCA of normalized spectral count

874 data of DAPs *vs* the mean of Ctl, and (**C**) enriched KEGG Pathways (KPs, blue), biological

875 processes (BPs, green), molecular functions (MFs, brown) and cellular components (CC, pink)

GO-terms in *D. polymorpha* exposed to CBZ (6.1 ± 0.2 µg L^{-1}, green), MeHg (460 ± 20 ng L^{-1}, purple), the co-exposure (CBZ+MeHg, cyan) and Ctl (red) at T24.

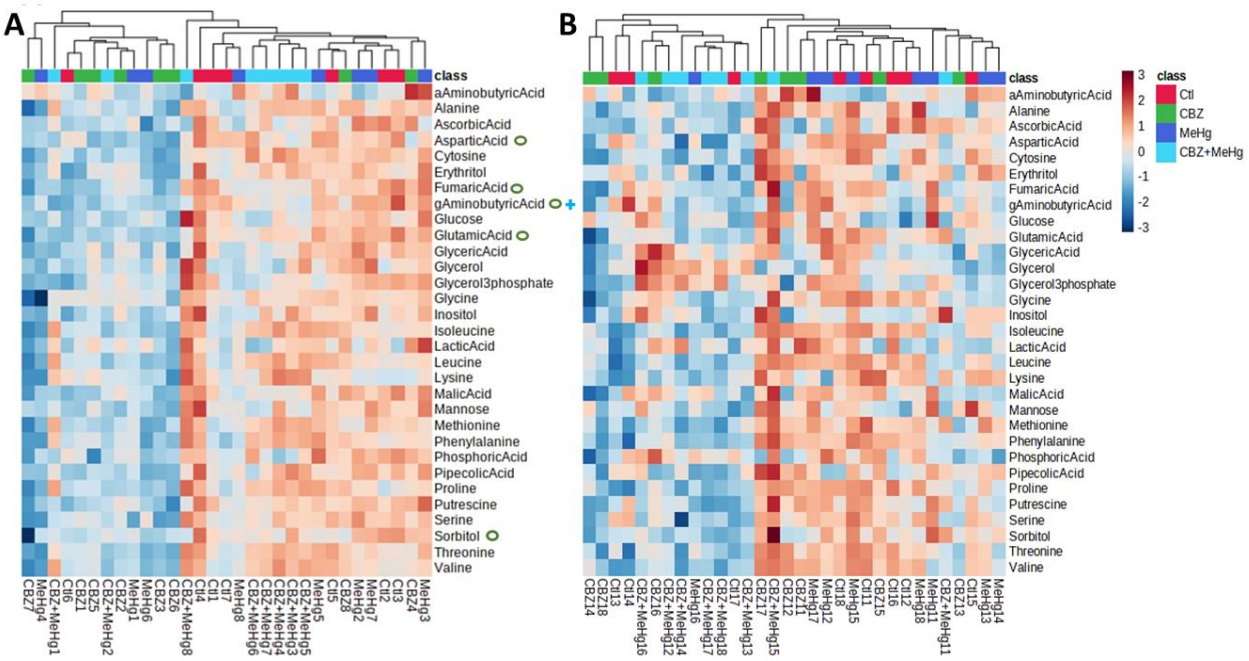

Figure 3: Heatmaps of the 31 quantified metabolites at T24 (**A**) and T72 (**B**) in *D. polymorpha* exposed to CBZ (6.1 ± 0.2 µg L^{-1}; green), MeHg (460 ± 20 ng L^{-1}; purple), the co-exposure (CBZ+MeHg; cyan), and Ctl (red) (n = 7 to 8). Modulated metabolites by CBZ (green circle) and the co-exposure (cyan cross) were identified by ANOVA analyses ($p<0.05$ and FC>1.4).

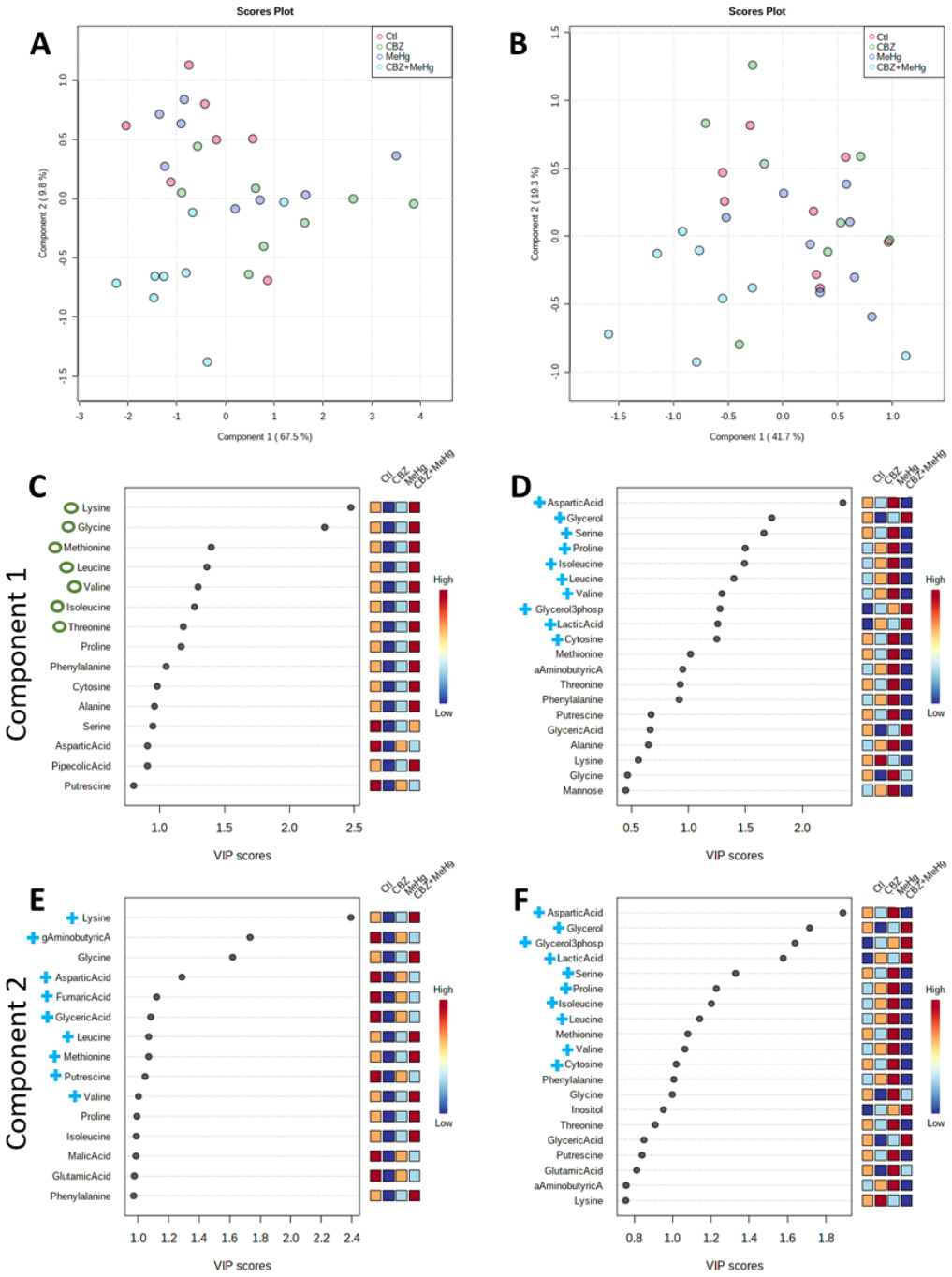

Figure 4: PLS-DAs (**A, B**) and VIP scores (**C** to **F**) of the 31 quantified metabolites at T24 (**A, C, E**) and T72 (**B, D, F**) in *D. polymorpha* exposed to CBZ (6.1 ± 0.2 µg L^{-1}; green), MeHg (460 ± 20 ng L^{-1}; purple), the co-exposure (CBZ+MeHg, cyan), and Ctl (red) (n = 7 to 8). Modulated metabolites in CBZ (green circle) and the co-exposure (cyan cross) were identified by multivariate analyses (VIP>1 and FC>1.4).

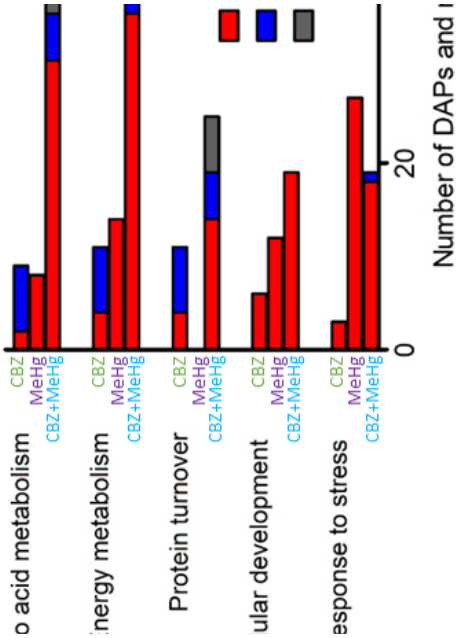

889

890 **Figure 5:** Number of significant modulations observed at proteome and metabolome levels in *D.*

891 *polymorpha* exposed to CBZ (6.1 ± 0.2 µg L^{-1}; green), MeHg (460 ± 20 ng L^{-1}; purple) and the

892 co-exposure (CBZ+MeHg, cyan) at T24 and T72. DAP = differentially abundant protein.

893

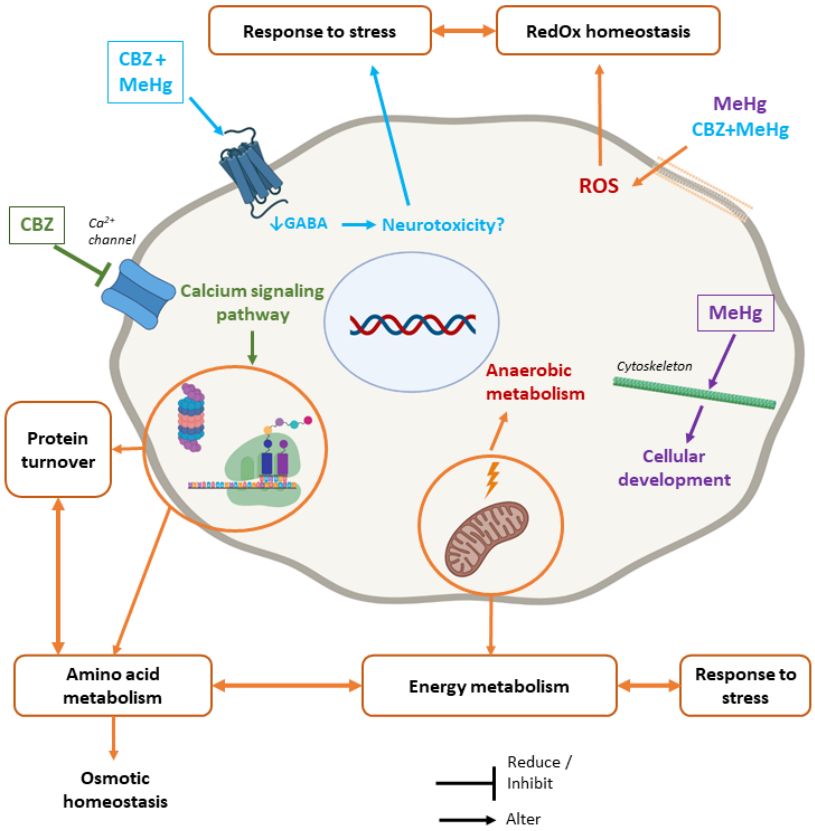

894

895 **Figure 6**: Main molecular responses observed in *D. polymorpha* exposed to CBZ (6.1 ± 0.2 µg L^{-1};

896 green), MeHg (460 ± 20 ng L^{-1}; purple), the co-exposure (cyan) and subsequent hypotheses.

897 Arrows in orange show common molecular toxicity pathways of single and co-exposures. ROS

898 = reactive oxygen species, GABA = ɣ-aminobutyric acid (designed with BioRender).